University of Alberta

Mass-Mobility Measurements of Aircraft Particulate Matter Using a Novel Measurement Method: A Centrifugal Particle Mass Analyzer and Differential Mobility Spectrometer System

by

Tyler James Johnson

A thesis submitted to the Faculty of Graduate Studies and Research
in partial fulfillment of the requirements for the degree of

Master of Science

Department of Mechanical Engineering

Fall 2013
Edmonton, Alberta

To Torbus Johnson

"Great Great Uncle Mike"

Radix Innovatione

Abstract

Mass-mobility measurements using a centrifugal particle mass analyzer (CPMA) and differential mobility spectrometer (DMS) are demonstrated. The CPMA, which classifies an aerosol by mass-to-charge ratio, is used upstream of a DMS, which measures the mobility size distribution of the mass-classified particles in real-time. Since the CPMA classifies particles by mass-to-charge ratio and multiply-charged particles are present, the particle mobility sizes of several different masses will be measured by the DMS. Therefore, a correction scheme is required to make accurate measurements. To validate this measurement scheme, two different CPMA-DMS systems were used to measure the known density of di(2ethylhexyl) sebacate (DEHS). The first system used a standard DMS500 (sDMS, Cambustion), while the second system used a modified DMS (mDMS), which had lower sizing uncertainties. The second configuration, a CPMA-mDMS system, was then used to measure the mass and mobility of aircraft particulate matter generated by CFM56-5B4-2P, CFM56-7B26 and PW4000-100 turbine engines.

Acknowledgements

I would like to thank my supervisor, Dr. Jason Olfert, for introducing me to research during my undergraduate degree. These experiences led me to pursue my Masters. I am grateful for all of the support and opportunities that he has provided me over the duration of my studies. I truly enjoyed my project and appreciate the countless hours he spent discussing the research, providing very helpful insights and reviewing my papers.

I also want to thank Dr. Jonathan Symonds from Cambustion. He was highly involved in my research to the point that he was basically a co-supervisor. I appreciate all of his help and guidance developing the CPMA-DMS correction process and the resulting papers from this research.

I would not have been able to compile the SAMPLE III results without the help of Dr. Mark Johnson from Rolls-Royce and Dr. Andrew Crayford from the University of Cardiff. I also appreciate the insights regarding the SAMPLE III data and its analysis from Dr. Kevin Thomson and Dr. Greg Smallwood from NRC and Dr. Jacob Swanson and Dr. Adam Boies from the University of Cambridge.

I would also like to acknowledge the financial support I received from GARDN, MDS Aero Support Corporation, NSERC, Alberta Innovates - Technology Futures, the University of Alberta, the Department of Mechanical Engineering, Prairie Mines and Royalty Ltd and the Alberta Government. This support allowed me to focus completely on my studies.

Finally I would like to thank my parents, Kris and Jim Johnson, and my girlfriend, Kimberley Watson, for their support over the years. Without them I would not be where I am today.

Contents

List of Tables

List of Figures

Chapter 1

Introduction

Over the last century the advancement of technology, particularly instrumentation, has led to the discovery and more accurate characterization of aerosols. Aerosols are small particles, usually in the nanometer to micrometer range, that are suspended in a gas medium. Some common examples of aerosols are dust, cigarette smoke or car exhaust. Particulate matter (PM) is a subcategory of aerosols and usually refers to aerosols of a carbonaceous nature, such as diesel engine or turbine engine exhaust.

1.1 Effects of particulate matter

Particulate matter adversely affects the environment by lowering air quality and visibility (Hinds, 1999). These particles are also small enough to deposit in the human lung or even translocate into the circulatory system, affecting human health (Pope, 2000). The global climate is also influenced by these emission sources as the particles scatter or absorb solar radiation or act as heterogeneous nucleation sites for clouds, affecting the radiative balance of heat within the atmosphere (Forster et al., 2007). Therefore, turbine engine PM emissions also negatively impact the environment (Unal et al., 2005; Woody et al., 2011), the global climate (Brasseur

A version or portion of this chapter has been submitted for publication/accepted for publication/published. Accepted: Johnson et al. (2013b), Submitted: Johnson et al. (2013a)

et al., 1998; Lee et al., 2009a) and human health (Ratliff et al., 2009). This emission source is only expected to grow as revenue passenger miles are predicted to increase an average of 2.2% per year domestically in the United States and 4.2% per year internationally over the next 20 years (FAA, 2013).

1.2 Particulate matter regulations

Particulate emissions are regulated and controlled in the interest of the public. The smoke number has been the standard emissions test of aircraft exhaust since the 1970's and ensures the exhaust is "non-visible" (SAE, 2011a). This property is quantified by measuring the relative optical reflectance of aircraft soot that has been collected on filter paper (SAE, 2011a). However this measurement is biased towards larger particles as light scattering is proportional to the particle diameter squared. Therefore this standard may or may not be a good metric for quantifying the health and climate effects of these emissions. Gas-phase emissions of aircraft exhaust, such as CO_2, CO and NO_x, have also been characterized since the 1970's following SAE ARP1256 (SAE, 2011b) and more recently SAE ARP1533 (SAE, 2013a). However these standards also do not account for the PM emissions component of aircraft exhaust. Therefore SAE has started developing additional standards to address these concerns. SAE AIR5892 (SAE, 2004) and AIR6037 (SAE, 2010) discuss the possible measurement methods that could be used to characterize aircraft PM. These documents led to the development of SAE AIR6241 (SAE, 2013b), which is currently in draft form. Similar to automotive standards (ISO, 2002), this standard proposes that aircraft PM emissions should be regulated based on non-volatile particle number and mass concentrations.

The effects of an emission source on human health and the climate are particle size dependent. Therefore both the particle number and mass concentrations are required to quantify this effect. A low mass concentration might meet emission standards, yet the source could still be harmful if the particle number concentration is high, indicating a significant amount of small particles with negligible mass.

Particle number concentration is usually measured by a condensation particle counter (CPC). This method condenses a liquid on the particles, such as butanol or water, to increase the particle size to the point that they can be detected and counted by an optical eye (Agarwal and Sem, 1980). The other most common method uses an electrometer to measure the charge concentration of the aerosol. This method requires the charge distribution of the aerosol to be known to convert the aerosol charge concentration to particle number concentration.

While many methods exist to measure PM mass concentration (SAE, 2010), such as gravimetric filters, thermo-optical methods (such as NIOSH 5040), tapered element oscillating microbalances (TEOM) or multiangle absorption photometry (MAAP), only two methodologies currently meet the requirements of SAE AIR6241 (SAE, 2013b). The laser induced incandescence (LII) heats the particles with a modulated laser and measures the incandescence signal produced by the particulate matter using two-color pyrometry (Snelling et al., 2000). This incandescence signal is proportional to the soot volume fraction (Melton, 1984). The micro soot sensor (MSS) or photoacoustic soot sensor (PASS) also uses a modulated laser to heat and cool the particulate matter (Schindler et al., 2004). This cycle causes the particles to expand and contract, thus generating pressure fluctuations or sound waves in the surrounding medium that can be detected by a microphone and are proportional to the soot concentration.

1.3 Mass-mobility relationship

Non-volatile aircraft emissions at the turbine engine exit plane consist mainly of black carbon aggregates (Anderson et al., 1998b; Timko et al., 2010; Peck et al., 2012) as shown in Figure 1-1.

Fractal-like aggregates are a formation of primary particles (Dobbins and Megaridis, 1987) and are often characterized by a power-law relationship (Schmidt-Ott et al., 1990; Koylu and Faeth, 1992; Faeth and Koylu, 1995; Sorensen, 2011). One way to define this correlation is the mass-mobility exponent (D_{m}). This parameter relates

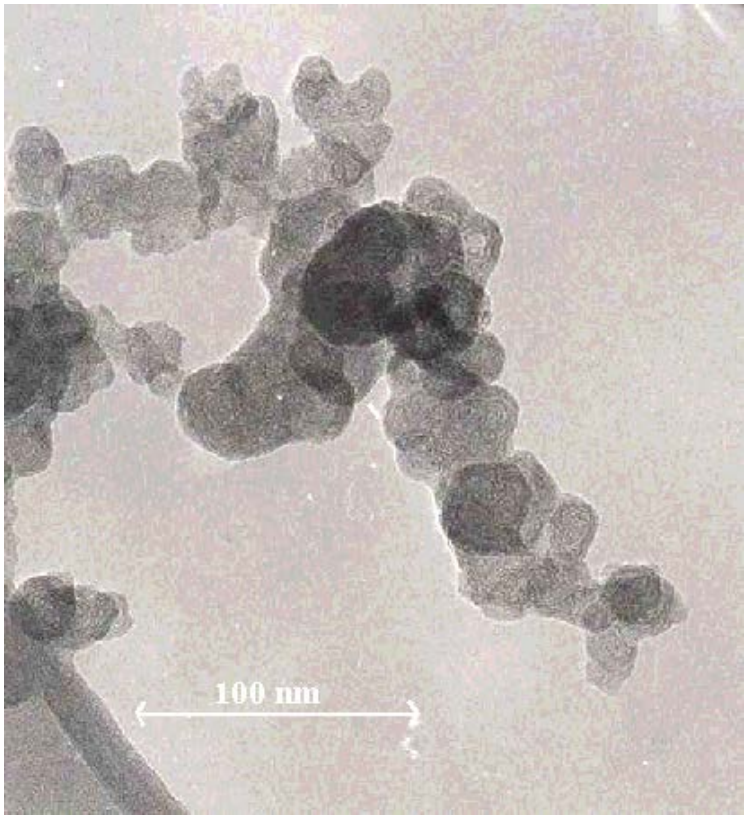

Figure 1-1: Transmission electron microscope (TEM) image of aircraft particulate matter (adapted from Johnson et al. (2003)).

the particle mass (m) to its mobility diameter (d_{m}) by:

$$m = C d_{\mathrm{m}}^{D_{\mathrm{m}}}, \tag{1.1}$$

where C is a constant[1]. The mobility diameter is the diameter of a sphere with the same electrical mobility or same dynamic behaviour when placed in an external electric field as the particle in question. This parameter is easy to measure using an electrostatic classifier, such as a differential mobility analyzer (DMA), and therefore is usually reported as the particle size.

McMurry et al. (2002) extended the power-law relationship one step further by defining the effective particle density (ρ_{eff}) as the mass of the particle divided by its

[1]This equation is purely empirical and does not apply to the mass-mobilities of all non-spherical particles, such as in the transition regime (slip regime effects) as outlined by Sorensen (2011).

mobility-equivalent volume or expressed mathematically as:

$$\rho_{\text{eff}} = \frac{6}{\pi}\frac{m}{d_{\text{m}}^3} = k d_{\text{m}}^{D_{\text{m}}-3}, \tag{1.2}$$

where k is a constant ($k = 6C/\pi$). This equation is typically fitted to mass-mobility results from combustion sources, such as flames (Maricq and Xu, 2004) and diesel engines (Park et al., 2004; Olfert et al., 2007), as these particles usually exhibit fractal-like properties.

Volatile material is also produced from turbine engines. This component of the exhaust is very sensitive to sampling or post mixing conditions as it easily condenses or evaporates at lower temperatures (<200°C). It is usually formed from gaseous combustion products, such as water vapor and organic hydrocarbons (Onasch et al., 2009; Beyersdorf et al., 2012), and/or fuel sulfur (Anderson et al., 1998a; Wey et al., 2007) condensing on the non-volatile components.

1.4 Applications of the mass-mobility relationships

Park et al. (2003b) and Liu et al. (2012) showed mass-mobility exponents or effective densities can be used to convert mobility-based size distributions to mass distributions, which can be integrated to calculate the total particulate mass concentration. This principle provides alternatives for traditional mass measurements, such as gravimetric filters and thermo-optical methods (NIOSH 5040), which require long samples times and therefore are not feasible for aircraft measurements. Furthermore mobility sizing instruments, such as a scanning mobility particle sizer (SMPS; Wang and Flagan, 1990), are able to detect single particles. Therefore very low mass concentrations can be measured with a mobility size distribution if the effective density function is known or measured, as shown in Figure 1-2.

Mass-mobility exponents and effective densities also provide a relationship between aerodynamic[2] and mobility sizes and information on particle morphology

[2]The aerodynamic diameter is the diameter of a sphere with unit density that has the same settling velocity as the particle in question.

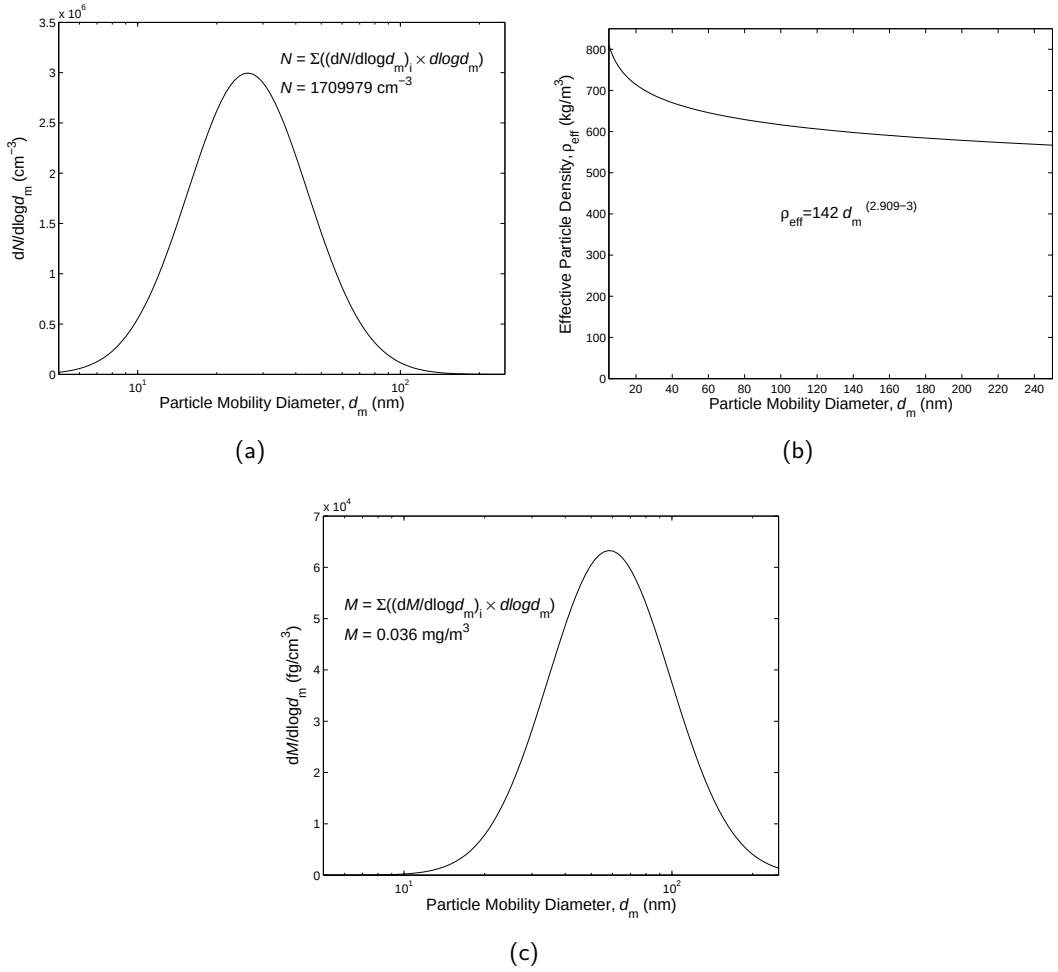

Figure 1-2: (a) Example of an aerosol mobility-size distribution, summing the size bins determines the total particle number concentration. (b) Example of an aerosol effective density function. (c) Mass distribution calculated from the example mobility-size distribution and effective density function, summing the size bins determines the total mass concentration.

(DeCarlo et al., 2004). Particle morphology is the structure or shape of the particle. This characteristic affects particle transportation and behaviour in the atmosphere (Jacobson, 2001) and human lung (Scheckman and McMurry, 2011; Rissler et al., 2012).

To calculate particulate matter (PM) mass emissions from measured mobility size distributions, previous turbine engines studies have assumed that aircraft exhaust particles were solid spheres that have unit density (Anderson et al., 2005; Wey et al., 2007; Kinsey, 2009; Mazaheri et al., 2009; Kinsey et al., 2012; Peck et al., 2012) or the density of carbon (1500-1900 kg/m^3) (Hagen et al., 1998; Lukachko et al., 2005; Brundish et al., 2007; Dakhel et al., 2007). The validity of these assumptions is questionable as the particles are expected to be nonspherical and follow a fractal-like relationship causing the effective density to be a function of the particle size. Therefore, having a known density function would avoid these assumptions and yield more accurate results.

1.5 Previous mass-mobility measurement techniques

Traditionally, the effective density is measured using a differential mobility analyzer (DMA), a mass analyzer and condensation particle counter (CPC) in series; where the mass-analyzer could be either a centrifugal particle mass analyzer (CPMA; Olfert et al., 2006) or an aerosol particle mass analyzer (APM; Ehara et al., 1996). A DMA selects particles based on their electrical mobility diameter using an electrostatic classifier as shown in Figure 1-3.

Particles are charged upstream of the electrostatic classifier using a radioactive neutralizer. A radioactive neutralizer charges particle by producing positive and negative ions or bipolar ions. These ions impact the particles through diffusion and the balance of these ions on each particle determines its charge state. This charged aerosol sample, as well as clean (particle free) sheath flow, are introduced at the top of the classifier as shown in Figure 1-3. A voltage potential is placed between the classifier's two concentric cylinders, inducing an electrostatic force on the charged

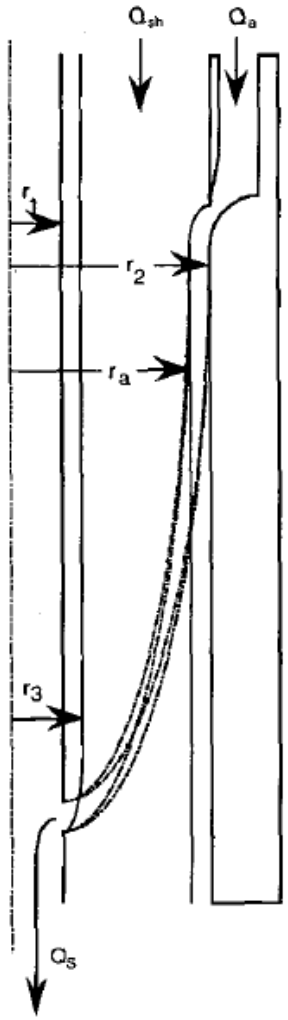

Figure 1-3: Schematic of DMA, where Q_{sh} is the sheath flowrate, Q_{a} is the inlet sample flowrate, Q_{s} is the outlet sample flowrate, r_1 is the radius of the inner cylinder or collection rod, r_2 is the radius of the outer cylinder and r_{a} is the minimum radius inlet position for a particle with the set mobility diameter that will allow it to pass though the classifier (adapted from Wang and Flagan (1990)).

particles in the radial direction of the classifier. This electrostatic force causes the particles to move relative to the surrounding gas medium, usually air, inducing a drag force on the particles against its relative motion. Therefore only particles that experience the correct drag and electrostatic forces or possessing the selected electrical mobility diameter will travel from the classifier sample inlet to outlet. Particles with smaller mobility diameters will impact and stick to the inner cylinder before reaching the outlet slot, while particles with larger mobility diameters will not reach the outlet slot in time and will be carried out through the bottom of the classifier with the sheath flow.

A CPMA classifies particles by their mass-to-charge ratio by balancing opposing electrostatic and centrifugal forces as shown in Figure 1-4.

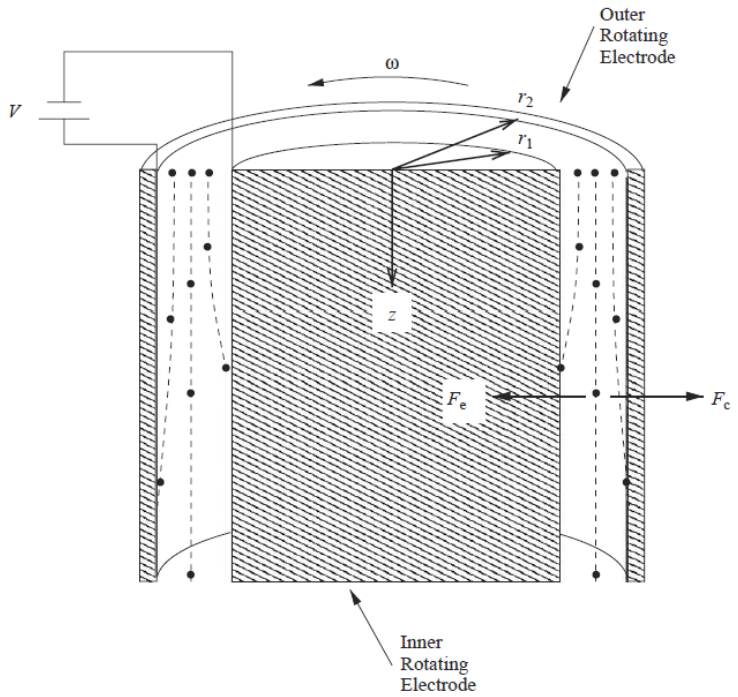

Figure 1-4: Schematic of CPMA, where r_1 is the radius of the inner cylinder, r_2 is the radius of the outer cylinder, ω is the angular velocity of the cylinders, V is the voltage potential between the cylinders, F_e is the particle electrostatic force and F_c is the particle centrifugal force (adapted from Olfert and Collings (2005)).

The electrostatic force (F_e) is generated by placing a voltage potential (V) between the two concentric cylinders, while the centrifugal force (F_c) is generated by spinning these cylinders. While both the CPMA and APM classify particles by their

mass-to-charge ratio by balancing opposing electrostatic and centrifugal forces, the CPMA's inner cylinder is spun slightly faster than the outer cylinder to generate Couette flow. This subtle difference from the APM's cylinders (which rotate at the same angular velocity) creates a stable system of forces on the particles, thereby improving the transmission efficiency of the CPMA over the APM (Olfert and Collings, 2005). For the remainder of this work the terms CPMA and APM are interchangeable as the proposed method was developed using a CPMA, but would also work with an APM.

The layout of the DMA-CPMA-CPC system is shown in 1-5.

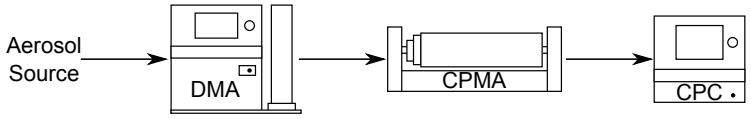

Figure 1-5: Schematic of DMA-CPMA-CPC system.

In this setup a DMA, with a charge neutralizer, is used to electrically charge and select the aerosol based on electrical mobility. The particles exiting the DMA will have a narrow range of electrical mobilities. However, due to the possibility of multiple-charge states, the particles will likely have different mechanical mobilities. The CPMA further classifies the particles by mass-to-charge ratio. The concentration of classified particles is measured by a condensation particle counter (CPC). By stepping the voltage and/or rotational speed of the CPMA, the aerosol concentration is recorded as a function of the CPMA operating condition. If no multiply-charged particles are present and the particles have a uniform effective density over the range of mobilities, then this function is approximately normally-distributed and the maximum corresponds to the average mass of the particles exiting the CPMA. Alternatively, if the resolution of the DMA and CPMA is sufficiently high, or the fraction of multiply-charged particles is sufficiently low, and the mass-to-charge ratio of the particles with equivalent electrical mobility are sufficiently different, then the multiply-charged particles are seen as separate maxima in the number concentration function. These maxima can be fit with a least squares minimization using an asymmetric normal distribution or a lognormal distribution as done by Tajima

et al. (2011) or by a function constructed by the convolution of the DMA and CPMA transfer functions (Emery, 2005; Barone et al., 2011). Otherwise other correction schemes are required (Olfert et al., 2007; Shin et al., 2009). This setup, using either a CPMA or APM, has been used to measure the effective density of diesel soot (Park et al., 2003a; Olfert et al., 2007; Barone et al., 2011), flame soot (Kim et al., 2009b; Xue et al., 2009; Cross et al., 2010; Ghazi et al., 2013), carbon nanofibres/nanotubes (Ku et al., 2006; Kim et al., 2009a), oils or secondary organic aerosols (SOA) (Malloy et al., 2009), metallic or silica agglomerates (Shin et al., 2009; Scheckman et al., 2009; Eggersdorfer et al., 2012), Aquadag and fullerene soot (Gysel et al., 2011) and nano-particles produced by spray-drying (Lee et al., 2009b, 2011).

Another method to determine the mass-mobility of aerosols uses a SMPS and electrical low pressure impactor (ELPI; Keskinen et al., 1992) in parallel. The mobility size distribution (measured by the SMPS) and aerodynamic diameter (measured by the ELPI) are related by the average effective density of the particles (Ahlvik et al., 1998). This method was used by Ristimaki et al. (2002) to measure particles of DOS, Santovac vacuum oil and Fomblin vacuum oil and by Virtanen et al. (2004) to measure DOS and silver agglomerate particles. A variation of this method places a DMA in series with an ELPI. This experimental set-up was used by Maricq and Xu (2004) to measure poly-α-olefin oil aerosol, diesel engine exhaust and direct injection spark ignition engine exhaust. Fernandez de la Mora et al. (2003) used a DMA and a focused impactor to measure the mobility and mass of silver particles with mobility diameters below 10 nm.

DeCarlo et al. (2004) also showed that the relationship between mobility and vacuum aerodynamic diameter can be used to determine the effective density of aerosol particles. A DMA or SMPS is used to classify/measure the particles based on electrical mobility, while the vacuum aerodynamic diameter is measured using an aerosol mass spectrometer (AMS; Jayne et al., 2000). Malloy et al. (2009) used the parallel combination of an SMPS and AMS to measure the effective density of SOA and this was compared against results obtained using a tandem APM-SMPS system, where the SMPS was scanned downstream of the APM operating at fixed

conditions.

The mass-mobility relationship can also be determined for very small particles (<3 nm) using a tandem DMA-mass spectrometer system, where the particle mass is directly measured by the mass spectrometer, as demonstrated by Larriba et al. (2011).

1.6 Aircraft particulate matter

Many studies have characterized aircraft exhaust using particle number concentrations (Anderson et al., 1998b; Corporan et al., 2007), mass concentration (Rogers et al., 2005; Cheng et al., 2008), gas phase emissions (Herndon et al., 2008; Spicer et al., 2009) or other characteristics (Wayson et al., 2002); however, only a few studies have measured effective density. Yu et al. (2010) measured the average effective density of turbine engine lubrication oil emissions to be 930 kg/m^3 using the relationship between particle vacuum aerodynamic diameter (measured using a compact time-of-flight aerosol mass spectrometer, C-TOFAMS) and volume equivalent diameter (measured using an ultra high sensitivity aerosol spectrometer, UHSAS). Using the same measurement principle Onasch et al. (2009), using an AMS and Scanning Mobility Particle Sizer (SMPS), measured the average effective density of the soot produced by a CFM56-2-C1 turbine engine at high throttle to be approximately 1000 kg/m^3. Li-Jones et al. (2007) also measured an average effective density of 1000 kg/m^3 from a T700 helicopter engine, using filters to determine the total particle mass and the measured size distribution to calculate the total particle volume. Timko et al. (2010) measured the effective densities from a PW308 turbine engine using two different methodologies. The first method, like the previous studies, determined the average effective density using an AMS and SMPS. This value was found to be between 400 kg/m^3 to 820 kg/m^3 depending on the type of fuel used and engine thrust. The second method determined the average effective density from the total particle mass measured using a multiangle absorption photometer (MAAP) and the total particle volume measured using an SMPS. This value was

found to range from 710 kg/m^3 to 840 kg/m^3 depending on the type of fuel used and engine thrust.

1.7 Overview

Although the DMA-CPMA-CPC system is relatively accurate (determined in Chapter 2 to be 9.4% in terms of effective density), the stepping aspect of this method limits its applications to steady state measurements. Chapter 2 explains how a CPMA and differential mobility spectrometer (DMS; Reavell et al. 2002; Biskos et al. 2005; Symonds et al. 2007) system, with a known or independently determined mobility size distribution, can measure the effective density of aerosol particles. In this system, the particles are neutralized by a radioactive source, classified by mass-to-charge ratio by the CPMA, and then the electrical mobilities of the mass-classified particles are measured in real-time with a DMS. Thus the effective density of one particle size can be measured in real-time, which is necessary for transient sources, or the effective density of several particle sizes can be measured in a few minutes from steady state sources. However these advantages come at the cost of uncertainty compared to the traditional DMA-CPMA-CPC system. This work also describes a correction scheme to account for the multiply-charged particles classified by the CPMA. Two DMS500 (Cambustion, U.K.) systems were tested, a standard DMS500 (sDMS) and a modified DMS500 (mDMS). The modified DMS had its charger disabled and flow rates dropped to decrease the mobility measurement uncertainty. These two CPMA-DMS systems were validated by measuring the effective density of di(2ethylhexyl) sebacate (DEHS).

Chapter 3 describes the mass-mobility distributions of aircraft exhaust particles measured using a CPMA-mDMS system. This system provides the size-resolved effective densities of particulate matter, allowing the nvPM mass concentration to be calculated from the measured non-volatile mobility size distribution. Thus one mobility-sizing instrument, such as a SMPS or DMS, could be used to complete both the number and mass concentration measurements required by current or proposed

regulations (SAE, 2013b). Previous aircraft effective density studies, as described above, measured the mass-weighted average effective density and therefore did not account for the change in effective density with particle mobility size when calculating the nvPM mass concentration. Furthermore the effects of sample dilution, a catalytic stripper (CS), engine type and thrust on the effective density functions are discussed. These results are also compared against other nvPM mass instruments, such as the laser-induced incandescence (LII, Artium Technologies Inc.) and micro soot sensor (MSS, AVL) by integrating the mobility size distributions, that were measured independently using a scanning mobility particle sizer (SMPS, TSI), with the effective density functions to determine the nvPM mass concentration.

Bibliography

Agarwal, J. K. and Sem, G. J. (1980). Continuous flow, single-particle-counting condensation nucleus counter. *Journal of Aerosol Science*, 11(4):343 – 357.

Ahlvik, P., Ntziachristos, L., Keskinen, J., and Virtanen, A. (1998). Real time measurements of diesel particle size distribution with an electrical low pressure impactor. Technical Report SAE 980410.

Anderson, B., Cofer, W., Barrick, J., Bagwell, D., and Hudgins, C. (1998a). Airborne observations of aircraft aerosol emissions ii: factors controlling volatile particle production. *Geophysical Research Letters*, 25(10):1693 – 1696.

Anderson, B. E., Branham, H. S., Hudgins, C. H., Plant, J. V., Ballenthin, J. O., Miller, T. M., Viggiano, A. A., Blake, D. R., Boudries, H., Canagaratna, M., Miake-Lye, R., Onasch, T. B., Wormhoudt, J., Worsnop, D. R., Brunke, K. E., Culler, S., Penko, P., Sanders, T., Han, H. S., Lee, P., Pui, D. Y. H., Thornhill, K. L., and Winstead, E. (2005). Experiment to characterize aircraft volatile aerosol and trace-species emissions (excavate). Technical report, National Aeronautics and Space Administration (NASA).

Anderson, B. E., Cofer, W. R., Bagwell, D. R., Barrick, J. W., Hudgins, C. H., and

Brunke, K. E. (1998b). Airborne observations of aircraft aerosol emissions i: Total nonvolatile particle emission indices. *Geophysical Research Letters*, 25(10):1689–1692.

Barone, T. L., Lall, A. A., Storey, J. M. E., Mulholland, G. W., Prikhodko, V. Y., Frankland, J. H., Parks, J. E., and Zachariah, M. R. (2011). Size-resolved density measurements of particle emissions from an advanced combustion diesel engine: effect of aggregate morphology. *Energy & Fuels*, 25(5):1978–1988.

Beyersdorf, A. J., Thornhill, K. L., Winstead, E. L., Ziemba, L. D., Blake, D. R., Timko, M. T., and Anderson, B. E. (2012). Power-dependent speciation of volatile organic compounds in aircraft exhaust. *Atmospheric Environment*, 61(0):275 – 282.

Biskos, G., Reavell, K., and Collings, N. (2005). Description and theoretical analysis of a differential mobility spectrometer. *Aerosol Science and Technology*, 39(6):527–541.

Brasseur, G., Cox, R., Hauglustaine, D., Isaksen, I., Lelieveld, J., Lister, D., Sausen, R., Schumann, U., Wahner, A., and Wiesen, P. (1998). European scientific assessment of the atmospheric effects of aircraft emissions. *Atmospheric Environment*, 32(13):2329–2418.

Brundish, K. D., Clague, A. R., Wilson, C. W., Miake-Lye, R. C., Brown, R. C., Wormhoudt, J., Lukachko, S. P., Chobot, A. T., Yam, C. K., Waitz, I. A., Hagen, D. E., Schmid, O., and Whitefield, P. D. (2007). Evolution of carbonaceous aerosol and aerosol precursor emissions through a jet engine. *Journal of Propulsion and Power*, 23(5):959–970.

Cheng, M.-D., Corporan, E., DeWitt, M. J., Spicer, C. W., Holdren, M. W., Cowen, K. A., Laskin, A., Harris, D. B., Shores, R. C., Kagann, R., and Hashmonay, R. (2008). Emissions of military cargo aircraft: Description of a joint field measurement strategic environmental research and development program. *Journal of the Air & Waste Management Association*, 58(6):787–796.

Corporan, E., DeWitt, M. J., Belovich, V., Pawlik, R., Lynch, A. C., Gord, J. R., and Meyer, T. R. (2007). Emissions characteristics of a turbine engine and research combustor burning a fischer-tropsch jet fuel. *Energy & Fuels*, 21(5):2615–2626.

Cross, E. S., Onasch, T. B., Ahern, A., Wrobel, W., Slowik, J. G., Olfert, J., Lack, D. A., Massoli, P., Cappa, C. D., Schwarz, J. P., Spackman, J. R., Fahey, D. W., Sedlacek, A., Trimborn, A., Jayne, J. T., Freedman, A., Williams, L. R., Ng, N. L., Mazzoleni, C., Dubey, M., Brem, B., Kok, G., Subramanian, R., Freitag, S., Clarke, A., Thornhill, D., Marr, L. C., Kolb, C. E., Worsnop, D. R., and Davidovits, P. (2010). Soot Particle Studies Instrument Inter-Comparison Project Overview. *Aerosol Science and Technology*, 44(8):592–611.

Dakhel, P. M., Lukachko, S. P., Waitz, I. A., Miake-Lye, R. C., and Brown, R. C. (2007). Postcombustion evolution of soot properties in an aircraft engine. *Journal of Propulsion and Power*, 23(5):942 – 948.

DeCarlo, P., Slowik, J., Worsnop, D., Davidovits, P., and Jimenez, J. (2004). Particle morphology and density characterization by combined mobility and aerodynamic diameter measurements. part 1: Theory. *Aerosol Science and Technology*, 38(12):1185–1205.

Dobbins, R. and Megaridis, C. (1987). Morphology of flame-generated soot as determined by thermophoretic sampling. *Langmuir*, 3(2):254 – 259.

Eggersdorfer, M., Grohn, A., Sorensen, C., McMurry, P., and Pratsinis, S. (2012). Mass-mobility characterization of flame-made zro2 aerosols: Primary particle diameter and extent of aggregation. *Journal of Colloid and Interface Science*, 387(1):12 – 23.

Ehara, K., Hagwood, C., and Coakley, K. (1996). Novel method to classify aerosol particles according to their mass-to-charge ratio - aerosol particle mass analyser. *Journal of Aerosol Science*, 27(2):217–234.

Emery, M. S. (2005). Theoretical analysis of data from dma-apm system. Master's thesis, Particle Technology Laboratory., Department of Mechanical Engineering, University of Minnesota, USA.

FAA (2013). Fact sheet - faa forecast for fiscal years 2013-2033.

Faeth, G. and Koylu, U. (1995). Soot morphology and optical properties in non-premixed turbulent flame environments. *Combustion science and technology*, 108(4-6):207 – 229.

Fernandez de la Mora, J., De Juan, L., Liedtke, K., and Schmidt-Ott, A. (2003). Mass and size determination of nanometer particles by means of mobility analysis and focused impaction. *Journal of Aerosol Science*, 34(1):79 – 98.

Forster, P., Ramaswamy, V., Artaxo, P., Berntsen, T., Betts, R., Fahey, D., Haywood, J., Lean, J., Lowe, D., Myhre, G., Nganga, J., Prinn, R., Raga, G., Schultz, M., and Van Dorland, R. (2007). *Climate Change 2007: The physical science basis*. Cambridge University Press, Cambridge, UK. Chapter 2.

Ghazi, R., Tjong, H., Soewono, A., Rogak, S. N., and Olfert, J. S. (2013). Mass, mobility, volatility, and morphology of soot particles generated by a mckenna and inverted burner. *Aerosol Science and Technology*, 47(4):395 – 405.

Gysel, M., Laborde, M., Olfert, J. S., Subramanian, R., and Grohn, A. J. (2011). Effective density of aquadag and fullerene soot black carbon reference materials used for sp2 calibration. *Atmospheric Measurement Techniques*, 4(12):2851 – 2858.

Hagen, D., Whitefield, P., Paladino, J., Trueblood, M., and Lilenfeld, H. (1998). Particulate sizing and emission indices for a jet engine exhaust sampled at cruise. *Geophysical Research Letters*, 25(10):1681–1684.

Herndon, S. C., Jayne, J. T., Lobo, P., Onasch, T. B., Fleming, G., Hagen, D. E., Whitefield, P. D., and Miake-Lye, R. C. (2008). Commercial aircraft engine emissions characterization of in-use aircraft at hartsfield-jackson atlanta international airport. *Environmental Science & Technology*, 42(6):1877–1883.

Hinds, W. C. (1999). *Aerosol technology- properties, behaviour and measurement of airborne particles*. John Wiley and Sons, 2nd edition.

ISO (2002). Heavy-duty engines- measurement of gaseous emissions from raw exhaust gas and of particulate emissions using partial flow dilution systems under transient test conditions. ISO16183.

Jacobson, M. (2001). Strong radiative heating due to the mixing state of black carbon in atmospheric aerosols. *Nature*, 409(6821):695–697.

Jayne, J., Leard, D., Zhang, X., Davidovits, P., Smith, K., Kolb, C., and Worsnop, D. (2000). Development of an aerosol mass spectrometer for size and composition analysis of submicron particles. *Aerosol Science and Technology*, 33(1-2):49–70.

Johnson, M. P., Hilton, M., Waterman, D. R., and Black, J. D. (2003). Development of techniques to characterize particulates emitted from gas turbine exhausts. *Measurement Science & Technology*, 14(7):1146.

Johnson, T., Olfert, J., Symonds, J. P., , Johnson, M., Swanson, J., Thomson, K., Smallwood, G. J., Crayford, A., and Boies, A. (2013a). Effective density and mass-mobility exponent of aircraft particulate matter. *Journal of Propulsion and Power*, In-preparation.

Johnson, T. J., Symonds, J. P., and Olfert, J. S. (2013b). Mass-mobility measurements using a centrifugal particle mass analyzer and differential mobility spectrometer. *Aerosol Science and Technology*, 47(11):1215–1225.

Keskinen, J., Pietarinen, K., and Lehtimaki, M. (1992). Electrical low-pressure impactor. *Journal of Aerosol Science*, 23(4):353–360.

Kim, S., Mulholland, G., and Zachariah, M. (2009a). Density measurement of size selected multiwalled carbon nanotubes by mobility-mass characterization. *Carbon*, 47(5):1297 – 1302.

Kim, S. C., Wang, J., Shin, W. G., Scheckman, J. H., and Pui, D. Y. H. (2009b). Structural Properties and Filter Loading Characteristics of Soot Agglomerates. *Aerosol Science and Technology*, 43(10):1033–1041.

Kinsey, J. S. (2009). Characterization of emissions from commercial aircraft engines during the aircraft particle emissions experiment (apex) 1 to 3. Technical report, U.S. Environmental Protection Agency.

Kinsey, J. S., Timko, M. T., Herndon, S. C., Wood, E. C., Yu, Z., Miake-Lye, R. C., Lobo, P., Whitefield, P., Hagen, D., Wey, C., Anderson, B. E., Beyersdorf, A. J., Hudgins, C. H., Thornhill, K. L., Edward, W., Howard, R., Bulzan, D. I., Tacina, K. B., and Knighton, W. B. (2012). Determination of the emissions from an aircraft auxiliary power unit (apu) during the alternative aviation fuel experiment (aafex). *Journal of the Air and Waste Management Association*, 62(4):420 – 430.

Koylu, U. and Faeth, G. (1992). Structure of overfire soot in buoyant turbulent diffusion flames at long residence times. *Combustion and Flame*, 89(2):140 – 156.

Ku, B. K., Emery, M. S., Maynard, A. D., Stolzenburg, M. R., and McMurry, P. H. (2006). In situ structure characterization of airborne carbon nanofibres by a tandem mobility-mass analysis. *Nanotechnology*, 17(14):3613–3621.

Larriba, C., Hogan, Jr., C. J., Attoui, M., Borrajo, R., Garcia, J. F., and de la Mora, J. F. (2011). The Mobility-Volume Relationship below 3.0 nm Examined by Tandem Mobility-Mass Measurement. *Aerosol Science and Technology*, 45(4):453–467.

Lee, D. S., Fahey, D. W., Forster, P. M., Newton, P. J., Wit, R. C., Lim, L. L., Owen, B., and Sausen, R. (2009a). Aviation and global climate change in the 21st century. *Atmospheric Environment*, 43(22-23):3520 – 3537.

Lee, S. Y., Chang, H., Ogi, T., Iskandar, F., and Okuyama, K. (2011). Measuring the effective density, porosity, and refractive index of carbonaceous particles by tandem aerosol techniques. *Carbon*, 49(7):2163 – 2172.

Lee, S. Y., Widiyastuti, W., Tajima, N., Iskandar, F., and Okuyama, K. (2009b). Measurement of the Effective Density of Both Spherical Aggregated and Ordered Porous Aerosol Particles Using Mobility- and Mass-Analyzers. *Aerosol Science and Technology*, 43(2):136–144.

Li-Jones, X., Penko, P. F., Williams, S., and Moses, C. (2007). Gaseous and particle emissions in the exhaust of a t700 helicopter engine. *Proceedings of the Asme Turbo Expo*, 2:395–411.

Liu, Z., Swanson, J., Kittelson, D. B., and Pui, D. Y. H. (2012). Comparison of methods for online measurement of diesel particulate matter. *Environmental Science & Technology*, 46(11):6127–6133.

Lukachko, S. P., Waitz, I. A., Miake-Lye, R. C., and Brown, R. C. (2005). Engine design and operational impacts on particulate matter precursor emissions. volume 2, pages 767 – 785.

Malloy, Q. G. J., Nakao, S., Qi, L., Austin, R., Stothers, C., Hagino, H., and Cocker, III, D. R. (2009). Real-Time Aerosol Density Determination Utilizing a Modified Scanning Mobility Particle Sizer-Aerosol Particle Mass Analyzer System. *Aerosol Science and Technology*, 43(7):673–678.

Maricq, M. and Xu, N. (2004). The effective density and fractal dimension of soot particles from premixed flames and motor vehicle exhaust. *Journal of Aerosol Science*, 35(10):1251 – 1274.

Mazaheri, M., Johnson, G. R., and Morawska, L. (2009). Particle and gaseous emissions from commercial aircraft at each stage of the landing and takeoff cycle. *Environmental Science & Technology*, 43(2):441–446.

McMurry, P., Wang, X., Park, K., and Ehara, K. (2002). The relationship between mass and mobility for atmospheric particles: A new technique for measuring particle density. *Aerosol Science and Technology*, 36(2):227–238.

Melton, L. (1984). soot Diagnostics Based On Laser-Heating. *Applied Optics*, 23(13):2201–2208.

Olfert, J. and Collings, N. (2005). New method for particle mass classification - the Couette centrifugal particle mass analyzer. *Journal of Aerosol Science*, 36(11):1338–1352.

Olfert, J. S., Reavell, K. S., Rushton, M. G., and Collings, N. (2006). The experimental transfer function of the Couette centrifugal particle mass analyzer. *Journal of Aerosol Science*, 37(12):1840–1852.

Olfert, J. S., Symonds, J. P. R., and Collings, N. (2007). The effective density and fractal dimension of particles emitted from a light-duty diesel vehicle with a diesel oxidation catalyst. *Journal of Aerosol Science*, 38(1):69–82.

Onasch, T. B., Jayne, J. T., Herndon, S., Worsnop, D. R., Miake-Lye, R. C., Mortimer, I. P., and Anderson, B. E. (2009). Chemical Properties of Aircraft Engine Particulate Exhaust Emissions. *Journal of Propulsion and Power*, 25(5):1121–1137.

Park, K., Cao, F., Kittelson, D. B., and McMurry, P. H. (2003a). Relationship between particle mass and mobility for diesel exhaust particles. *Environmental Science & Technology*, 37(3):577–583.

Park, K., Kittelson, D. B., and McMurry, P. H. (2003b). A closure study of aerosol mass concentration measurements: comparison of values obtained with filters and by direct measurements of mass distributions. *Atmospheric Environment*, 37:1223 – 1230.

Park, K., Kittelson, D. B., and McMurry, P. H. (2004). Structural properties of diesel exhaust particles measured by transmission electron microscopy (tem): Relationships to particle mass and mobility. *Aerosol Science and Technology*, 38(9):881 – 889.

Peck, J., Timko, M. T., Yu, Z., Wong, H.-W., Herndon, S. C., Yelvington, P. E., Miake-Lye, R. C., Wey, C., Winstead, E. L., Ziemba, L. D., and Anderson, B. E. (2012). Measurement of volatile particulate matter emissions from aircraft engines using a simulated plume aging system. *Journal of Engineering for Gas Turbines and Power*, 134(6).

Pope, C. A. (2000). Review: Epidemiological basis for particulate air pollution health standards. *Aerosol Science and Technology*, 32(1):4–14.

Ratliff, G., Sequeira, C., Waitz, I., Ohsfeldt, M., Thrasher, T., Graham, M., and Thompson, T. (2009). Aircraft impacts on local and regional air quality in the united states. Technical report, Partnership for AiR Transportation Noise and Emissions Reduction (PARTNER).

Reavell, K., Hands, T., and Collings, N. (2002). A fast response particulate spectrometer for combustion aerosols. Technical Report SAE 2002-01-2714.

Rissler, J., Swietlicki, E., Bengtsson, A., Boman, C., Pagels, J., Sandstrom, T., Blomberg, A., and Londahl, J. (2012). Experimental determination of deposition of diesel exhaust particles in the human respiratory tract. *Journal of Aerosol Science*, 48:18–33.

Ristimaki, J., Virtanen, A., Marjamaki, M., Rostedt, A., and Keskinen, J. (2002). On-line measurement of size distribution and effective density of submicron aerosol particles. *Journal of Aerosol Science*, 33(11):1541–1557.

Rogers, F., Arnott, P., Zielinska, B., Sagebiel, J., Kelly, K. E., Wagner, D., Lighty, J. S., and Sarofim, A. F. (2005). Real-time measurements of jet aircraft engine exhaust. *Journal of the Air & Waste Management Association*, 55(5):583–593.

SAE (2004). Nonvolatile exhaust particle measurement techniques. AIR5892.

SAE (2010). Aircraft exhaust nonvolatile particle matter measurement method development. AIR6037.

SAE (2011a). Aircraft gas turbine engine exhaust smoke measurement. ARP1179.

SAE (2011b). Procedure for the continuous sampling and measurement of gaseous emissions from aircraft turbine engines. ARP1256.

SAE (2013a). Procedure for the analysis and evaluation of gaseous emissions from aircraft engines. ARP1533.

SAE (2013b). Procedure for the continuous sampling and measurement of non-volatile particle emissions from aircraft turbine engines. AIR6241.

Scheckman, J. H. and McMurry, P. H. (2011). Deposition of silica agglomerates in a cast of human lung airways: Enhancement relative to spheres of equal mobility and aerodynamic diameter. *Journal of Aerosol Science*, 42(8):508–516.

Scheckman, J. H., McMurry, P. H., and Pratsinis, S. E. (2009). Rapid Characterization of Agglomerate Aerosols by In Situ Mass-Mobility Measurements. *Langmuir*, 25(14):8248–8254.

Schindler, W., Haisch, C., Beck, H. A., Niessner, R., Jacob, E., and Rothe, D. (2004). A photoacoustic sensor system for time resolved quantification of diesel soot emissions. Technical report.

Schmidt-Ott, A., Baltensperger, U., Gaeggeler, H., and Jost, D. (1990). Scaling behaviour of physical parameters describing agglomerates. *Journal of Aerosol Science*, 21(6):711 – 717.

Shin, W. G., Mulholland, G. W., Kim, S. C., Wang, J., Emery, M. S., and Pui, D. Y. H. (2009). Friction coefficient and mass of silver agglomerates in the transition regime. *Journal of Aerosol Science*, 40(7):573–587.

Snelling, D. R., Smallwood, G. J., Sawchuk, R. A., Neill, W. S., Gareau, D., Clavel, D. J., Chippior, W. L., Liu, F., Gulder, O. L., and Bachalo, W. D. (2000). In-situ real-time characterization of particulate emissions from a diesel engine exhaust by laser-induced incandescence. Technical report.

Sorensen, C. (2011). The mobility of fractal aggregates: A review. *Aerosol Science and Technology*, 45(7):755 – 769.

Spicer, C. W., Holdren, M. W., Cowen, K. A., Joseph, D. W., Satola, J., Goodwin, B., Mayfield, H., Laskin, A., Lizabeth Alexander, M., Ortega, J. V., Newburn, M., Kagann, R., and Hashmonay, R. (2009). Rapid measurement of emissions from military aircraft turbine engines by downstream extractive sampling of aircraft on the ground: Results for c-130 and f-15 aircraft. *Atmospheric Environment*, 43(16):2612–2622.

Symonds, J. P. R., Reavell, K. S. J., Olfert, J. S., Campbell, B. W., and Swift, S. J. (2007). Diesel soot mass calculation in real-time with a differential mobility spectrometer. *Journal of Aerosol Science*, 38(1):52–68.

Tajima, N., Fukushima, N., Ehara, K., and Sakurai, H. (2011). Mass range and optimized operation of the aerosol particle mass analyzer. *Aerosol Science and Technology*, 45(2):196–214.

Timko, M., Yu, Z., Onasch, T., Wong, H.-W., Miake-Lye, R., Beyersdorf, A., Anderson, B., Thornhill, K., Winstead, E., Corporan, E., Dewitt, M., Klingshirn, C., Wey, C., Tacina, K., Liscinsky, D., Howard, R., and Bhargava, A. (2010). Particulate emissions of gas turbine engine combustion of a fischer-tropsch synthetic fuel. *Energy and Fuels*, 24(11):5883 – 5896.

Unal, A., Hu, Y., Chang, M., Odman, M., and Russell, A. (2005). Airport related emissions and impacts on air quality: Application to the Atlanta International Airport. *Atmospheric Environment*, 39(32):5787–5798.

Virtanen, A., Ristimaki, J., and Keskinen, J. (2004). Method for measuring effective density and fractal dimension of aerosol agglomerates. *Aerosol Science and Technology*, 38(5):437–446.

Wang, S. and Flagan, R. C. (1990). Scanning electrical mobility spectrometer. *Aerosol Science and Technology*, 13(2):230–240.

Wayson, R. L., Fleming, G. G., and Kim, B. (2002). A review of literature on particulate matter emissions from aircraft. Technical report, Federal Aviation Administration.

Wey, C. C., Anderson, B. E., Wey, C., Miake-Lye, R. C., Whitefield, P., and Howard, R. (2007). Overview on the aircraft particle emissions experiment. *Journal of Propulsion and Power*, 23(5):898 – 904.

Woody, M., Baek, B. H., Adelman, Z., Omary, M., Lam, Y. F., West, J. J., and Arunachalam, S. (2011). An assessment of Aviation's contribution to current and future fine particulate matter in the United States. *Atmospheric Environment*, 45(20):3424–3433.

Xue, H., Khalizov, A. F., Wang, L., Zheng, J., and Zhang, R. (2009). Effects of Coating of Dicarboxylic Acids on the Mass-Mobility Relationship of Soot Particles. *Environmental Science & Technology*, 43(8):2787–2792.

Yu, Z., Liscinsky, D. S., Winstead, E. L., True, B. S., Timko, M. T., Bhargava, A., Herndon, S. C., Miake-Lye, R. C., and Anderson, B. E. (2010). Characterization of Lubrication Oil Emissions from Aircraft Engines. *Environmental Science & Technology*, 44(24):9530–9534.

Chapter 2

Mass-mobility measurements using a centrifugal particle mass analyzer and differential mobility spectrometer

2.1 Experimental set-up

The CPMA-DMS system is shown in Figure 2-1. For the specific example data shown in Chapter 2, the aerosol was DEHS droplets suspended in nitrogen, generated by atomizing a solution of 2-propanol (HPLC grade) with 0.1% volume concentration DEHS using a BGI 3-Nozzle Collison Nebuliser. A radioactive neutralizer is used to charge the aerosol as a prerequisite for CPMA classification. The CPMA (Cambustion, U.K.) is set to a constant mass-to-charge setpoint (i.e. constant rotational speed and voltage) and the mobility size distribution of the classified aerosol is measured by a DMS. A CPMA classifies individual aerosol particles by their mass-to-charge ratio by balancing opposing electrostatic and centrifugal forces. The electrostatic force is generated by charging the particles upstream of the CPMA and placing

A version or portion of this chapter has been submitted for publication/accepted for publication/published. Accepted: Johnson et al. (2013)

a voltage potential across the CPMA's inner and outer cylinders. The centrifugal force is generated by spinning the cylinders.

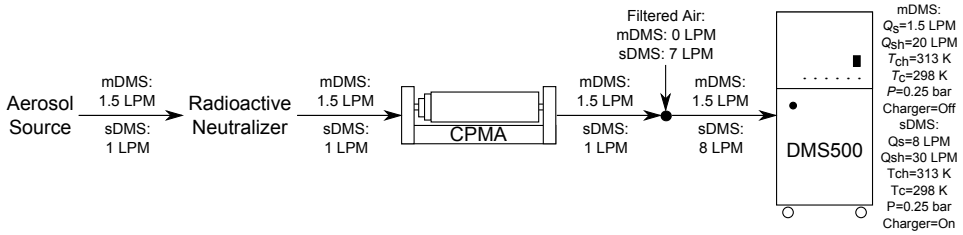

Figure 2-1: Experimental set-up for neutralizer-CPMA-DMS system where: Q_{s} is the DMS classifier sample flow rate, Q_{sh} is the DMS classifier sheath flow rate, T_{ch} is the DMS charger temperature, T_{c} is the DMS classifier temperature and P is the DMS classifier pressure.

A DMS measures the real-time mobility size distribution of an aerosol by classifying particles using electrical mobility. A corona charger is used to charge the aerosol particles before entering the DMS classifier. The classifier consists of two concentric cylinders with a potential difference between them. Similar to a DMA, the motion of charged particles in an electric field is dependent on their electrical mobility, and hence their electrical mobility diameter. These mobility paths are measured by electrometer rings, placed on the inner face on the outside classifier cylinder. These rings count the number of charges that fall into each electrical mobility bin by measuring the current generated by charged particles grounding on the electrometer rings. An inversion algorithm then converts these ring currents into an electrical mobility size spectral density plot.

Standard vs. Modified DMS

Two different DMS500 configurations were used in this study; a standard DMS (sDMS) and modified DMS (mDMS). The sDMS unipolar charging process has higher uncertainties at smaller particles sizes (0–100 nm) and is dependent on particle morphology (Symonds and Reavell, 2007; Symonds, 2010). Therefore, the mDMS had its charger disabled to improve its measurement uncertainty. Without the charger, the aerosol had lower electrical mobility and required a longer flight-time in the column to be classified. Therefore the sample flow rate was dropped

from 8 SLPM to 1.5 SLPM and the sheath flow rate was dropped from 30 SLPM to 20 SLPM, increasing the particle residence time. The lower sample flow rate also allowed direct sampling of the CPMA classified aerosol without make-up air, as it is designed for 1.5 LPM, and lower flow rates are generally desired for higher resolution at lower rotational speeds.

However these modifications limited the mDMS sizing range to 10–120 nm and reduced the current signal from the mDMS electrometer rings significantly. The inversion matrix used with the mDMS assumed all the particles were singly-charged. This assumption amplified the error from existing multiply-charged particles as a particle with n charges produced n times the current compared to a particle with 1 charge, making the mDMS measure n times the actual particle concentration. However, this amplification effect in the mDMS was accounted for within the correction method. This effect was accounted for in the sDMS by the inversion matrix considering the particle charge distribution leaving the sDMS corona charger. The inversion matrix used with the mDMS also produced 64 size-classes per decade, compared with the sDMS which had the standard 16 size-classes per decade.

2.2 Theory

2.2.1 Effects of uncharged particles

In a CPMA an uncharged particle experiences no electrostatic force and the centrifugal force is directly proportional to its mass. Therefore, if the particle has an extremely small mass, the centrifugal force is insufficient for classification to occur over its residence time in the CPMA. As a result, uncharged particles below a cutoff mass (which is dependent on the rotational speed of the cylinders) will pass through the CPMA. This cutoff mass was determined by calculating the CPMA transfer function in the absence of the electrostatic force (i.e. when the particles only experience centrifugal forces and diffusion). Further details regarding the CPMA cutoff mass and its calculation are outlined in Symonds et al. (2013).

Uncharged particles are not measured by the modified DMS and therefore a cor-

rection for uncharged particles is not required. However the corona charger in the standard DMS charges the uncharged particles affecting the mobility size distribution it measures. Standard DMS data can be corrected for uncharged particles in two ways:

(I) Manually setting the DMS ring currents generated by uncharged particles to a value of zero "by eye".

(II) Calculating the theoretical DMS ring currents generated by the uncharged particles and removing these currents from the measured currents.

Lower DMS ring numbers measure particles with higher mobilities or smaller mobility-equivalent diameters. Therefore the uncharged particles, which are always smaller than the classified particles, generate current on the lower DMS ring numbers, which usually makes the DMS ring current distribution bimodal, as shown in Figure 2-2.

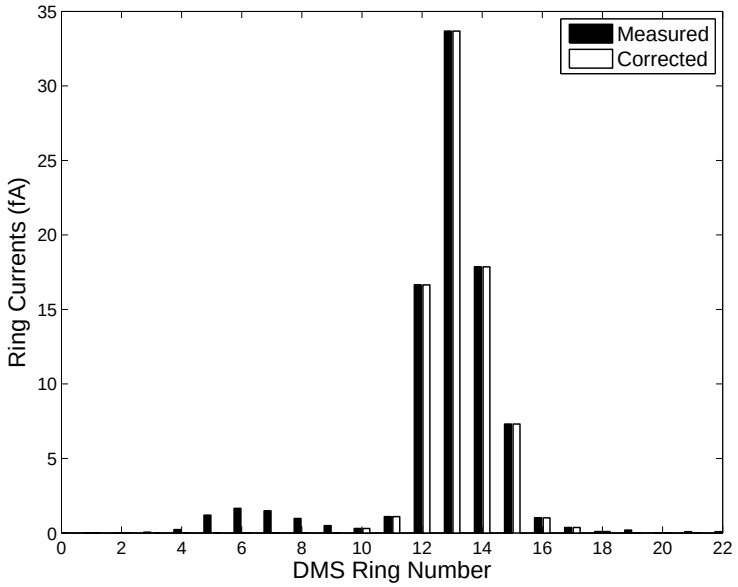

Figure 2-2: Example of ring currents generated by CPMA-sDMS measurements where the uncharged particles and CPMA-classified particle are distinguishable and the ring current due to the uncharged particles has been set to zero.

Therefore, Method (I) works well when there is a clear distinction between these modes or the DMS ring currents generated by the uncharged particles versus the classified particles. The effects of uncharged particles vary from being insignificant to

generating a majority of the DMS ring currents, depending on the CPMA rotational speed, mobility size and concentration of the aerosol being classified and the CPMA mass-to-charge setpoint.

While Method (I) is computationally faster, it does not work when the current generated by the uncharged particles and the classified particles are detected on common DMS rings as shown in Figure 2-3.

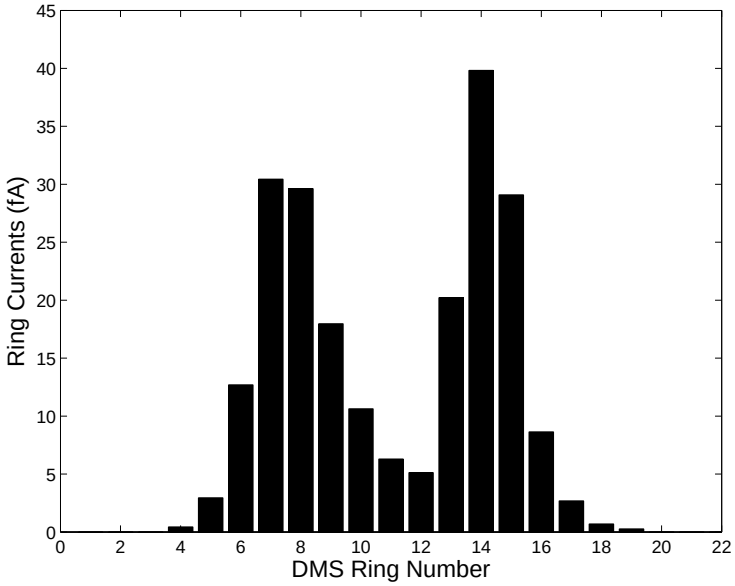

Figure 2-3: Example of ring currents generated by CPMA-sDMS measurements where the uncharged particles and CPMA-classified particles are not distinguishable.

Therefore, Method (II) must be applied to find and remove the current on each DMS ring generated from uncharged particles. The effect of uncharged particles in a standard DMS can be minimized by operating the CPMA at a higher resolution, which in turn classifies particles at a higher rotation speed, or setting the CPMA mass-to-charge setpoint to select from the leading edge (the smaller particle side) of the particle size distribution.

2.2.2 Neutralizer-CPMA-DMS system density function scan time

The time to measure a complete density distribution depends on how long it takes the CPMA to stabilize at each CPMA setpoint, how long the CPMA is stable at each setpoint, and how many points are measured along the density distribution.

While it is possible to scan just the voltage of the CPMA over a narrow mass range, the voltage and rotational speed of the CPMA are usually counter-scanned when scanning over a large mass range, to maintain a constant classifier resolution. This then increases the stabilisation time between points due to the acceleration or deceleration of the CPMA. It took just over 6 minutes to measure 16 points on the density distribution between 20 nm and 120 nm with the CPMA stabilizing for 5 s (2 s delay and 3 s averaging) at each setpoint.

2.2.3 DMS ring current correction method

An iterative scheme was used to correct the effective density measurements for multiply-charged particles for both the standard and modified DMS. The correction code was developed in Matlab R2012a and considers the effects of particle diffusion in both the CPMA and DMS. The code can be downloaded at www.cambustion.com/cpma. The Matlab CPMA diffusive transfer function was developed by Olfert and Collings (2005) and the Matlab DMS diffusive transfer function was developed by Cambustion (2011).

The following steps outline the method used for the multiple-charge correction as shown in Figure 2-4. If necessary the DMS ring currents can be corrected for noise before applying the multiple-charge correction. Noise removal and re-inversion is required at lower aerosol concentrations, especially for the modified DMS as the DMS corona charger is disabled resulting in lower currents. For example, the classified particles could generate current on DMS rings 5–10, however ring 21 could also be detecting a small amount of current. This lone ring current is extremely unlikely to be generated physically as even a monodispersed particle distribution has a distribution of charges and starting points at the DMS classifier inlet. Therefore, DMS ring currents are usually generated on multiple consecutive rings and any lone, isolated ring current is likely instrument noise. In such a case, the current on ring 21 would be set to zero and the DMS measured mobility size distribution recalculated.

An initial guess for the effective density of the aerosol is made for the CPMA diffusive model. This guess is required as the width of the CPMA transfer function,

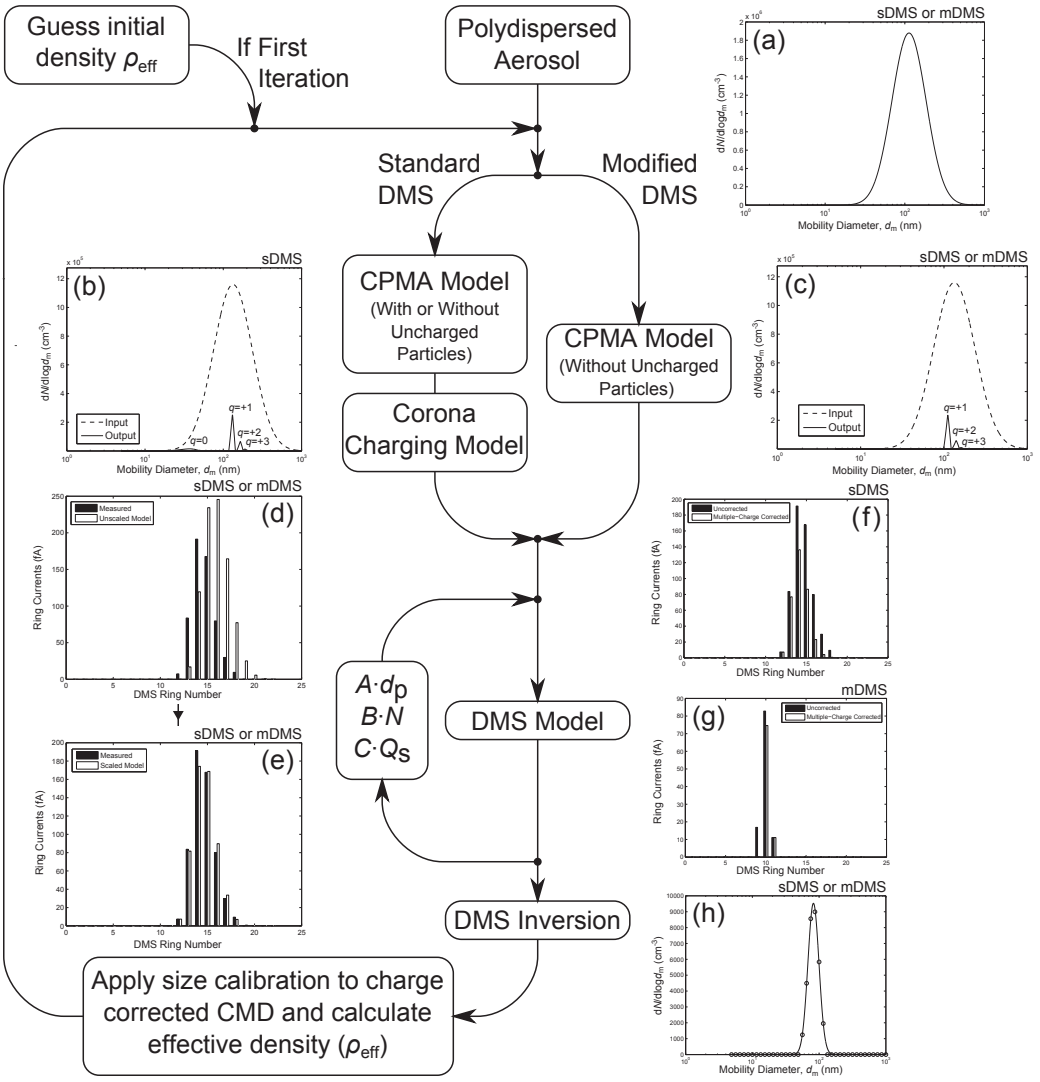

Figure 2-4: Correction method to remove the effects of multiply-charged particles and apply the size calibration to CPMA-DMS measurements. The sub-figures illustrate the results for one data point and depict the: (a) unclassified aerosol mobility size distribution, (b) CPMA classified mobility size distribution including uncharged particles, (c) CPMA classified mobility size distribution, (d) unscaled DMS model ring currents, (e) scaled DMS model ring currents, (f) multiply-charged corrected standard DMS ring currents, (g) multiply-charged corrected modified DMS ring currents, (h) multiply-charged corrected size distribution fitted with a lognormal distribution.

also referred to as the CPMA resolution, is dependent on particle mobility and this is the reason the correction process is iterative. The correction process allows a user defined initial guess, using either a constant density or power law density distribution, or for the guess to be calculated for each CPMA mass-to-charge setpoint using the uncorrected (no multiple-charge correction or size calibration applied) measured DMS count median diameter (CMD). The effective densities are fitted with a density function with the functional form shown in Equation 1.2. For each CPMA mass-to-charge setpoint the diffusive CPMA transfer function is calculated using the density function. This transfer function is applied to the polydispersed aerosol, which has to be measured independently of the CPMA-DMS system (using for example a DMS or SMPS), as shown in Figure 2-4a. These calculations determine the mobility size and number of particles that were classified by the CPMA for each particle charge state. Figure 2-4b shows the mobility size distribution of the aerosol exiting the CPMA for the standard DMS including uncharged particles, while Figure 2-4c shows the mobility size distribution of the aerosol exiting the CPMA for the modified DMS or the standard DMS with no uncharged particles. If an APM was used instead of a CPMA, the only modification to the current correction scheme would be applying the APM transfer function rather than the CPMA transfer function.

The model assumes the polydispersed aerosol has an equilibrium bipolar charge distribution using either the method described by Wiedensohler (1988) or Gopalakrishnan et al. (2013). When the elemental charge state considered is greater than 2 or less than -2 (the limits of these models) the equilibrium charge fraction is determined using Gunn and Woessner (1956). The Wiedensohler model is commonly used in aerosol sciences and was developed using Fuchs (1963) flux-matching theory and fitting the coefficients with a least-square regression analysis. The Gopalakrishnan et al. model uses the Brownian/Langevin dynamics to determine the equilibrium charge distribution over the entire Knudsen number range or for all regimes.

The model allows the user to specify the number of charge states that are classified by the CPMA. For the results shown 1 to 6 elemental charges were considered by the CPMA transfer function. These limits on the number of elemental charge

states were determined by running the model with increasing charge states and establishing when the results became independent of this parameter.

For the standard DMS, a corona or unipolar charging model is applied to determine the new charge states of the classified particles. This model was developed by Cambustion and allows the user to calculate the particle charging based on White (1951) or Fuchs (1963). The White model considers particle charging to occur through electric field charging for particles larger than 0.5 μm or ion diffusion for smaller particles, but does not account for both mechanisms simultaneously. White also assumes that the ion concentration is uniform and that the particles are in the free molecular regime and spherical. The Fuchs model calculates the unipolar charge distribution using flux matching theory and applies the limited sphere method to approximate ion capture in the transition regime. Fuchs also assumes the particles are spherical and neglects image potential.

The corona charger generates a charge distribution for each particle mobility size. Based on Fuch's charging model a 100 nm particle has a 14.11% probability of having 3 elemental charges, 48.49% of having 4 charges, 31.61% of having 5 charges, 5.15% of having 6 charges and 0.64% of having other charge states. The correction code for the standard DMS has the option to use the entire charge distribution or the average charge state. The average charge state (DMS Model 2) is the mean number of elemental charges on a particle at one particular mobility size (for example, the 100 nm particle mentioned above has a mean charge state of 3.96 elementary charges). The entire charge distribution can be implemented in two ways. The first method (DMS Model 1) applies the charge probabilities to each CPMA classified mobility size, determining the particle concentration for each particle mobility size and charge state. The second method (DMS Model 3) applies the charge distribution within the diffusive DMS model, and selects which bins to calculate based on the probability of each charge state. Therefore if sufficient iterations are selected DMS model 3 and DMS model 1 should agree. All of these DMS models apply the same DMS diffusive transfer function and any of the unipolar charger models implemented; the variation between them is the number of bins considered in the calculation and how

these bins are generated in an effort to reduce computation requirements. Therefore the diffusive DMS transfer function is applied based on the DMS model selected and determines the amount of theoretical current generated on each DMS ring. The theoretical ring currents are then compared against the measured ring currents as shown in Figure 2-4d.

The measured and theoretical currents do not always agree due to uncertainties in measured parameters or the theoretical models[1]. The charging model is the highest source of uncertainty as particle charging depends on its morphology, which is usually unknown. There are also uncertainties in system flows as the DMS does not measure the sample flow in real-time, but only when zeroing the instrument. Furthermore, the charging model does not account for the penetration efficiency of the corona charger used in the sDMS. Finally, both the CPMA and DMS models do not account for particles losses in the inlets and outlets of each instrument. Therefore, the disagreement between the measured and theoretical ring currents is minimized by using the Matlab function `fmincon` and:

- Applying a factor A to the mobility size of the classified particles, which shifts the peak of the theoretical currents along the DMS rings.
- Applying a factor B to the concentration of the classified particles, which scales the amplitude of the theoretical ring currents.
- Applying a factor C to the sample flow rate of the DMS, but keeping the sum of the DMS sample flow rate and sheath flow rate a constant. This scales the width of the DMS transfer function or the width of rings that the particles land on, but keeps C independent of B.

Constrained minimization is used to limit the scaling factors within a user specified tolerance of the measured values and avoids the generation of unrealistic factors. This principle is also applied to every other fitting scheme in the code; for example the mass-mobility exponent for the density function fit was limited between 1 and

[1]The commercial DMS500 is empirically calibrated with aerosols of a known size and concentration.

3 for these results. After the scaling factors are determined through constrained minimization, as shown in Figure 2-4e, the current generated by multiply-charged particles and uncharged particles (if considering that particular case for the standard DMS) is subtracted from the measured ring currents. Figure 2-4f shows the multiple-charge corrected ring currents for the standard DMS, while Figure 2-4g shows the multiple-charge corrected ring currents for the modified DMS. As expected the current is removed from the larger ring numbers for the standard DMS, but is removed from the smaller ring numbers for the modified DMS. This difference is due to the corona charger in the standard DMS which changes the electrical mobility of the CPMA classified particles.

Since the minimization applies linear scaling factors to a non-linear system not every data point agrees with the theoretical model. This disagreement is measured by the difference between the percent of current that should be removed from the DMS ring currents and the percent of current that is actually removed by the model. The percent of current that should be removed is calculated using the theoretical CPMA classified mobility size distribution and is the sum of each particle concentration times its charge state divided by the concentration of singly-charged particles. If the experimental data and theoretical model agree perfectly this difference is zero.

Next the corrected ring currents are re-inverted to a mobility size distribution using the DMS inversion matrix and fitted with a lognormal distribution as shown in Figure 2-4h. The CMD from the lognormal fit is corrected with one of the size calibration curves. Using the multiple-charge and size calibrated CMD and the CPMA mass-to-charge setpoint the corrected effective density is calculated and used as the guess for the next iteration. The difference between the current and previous iteration effective density is determined for each data point and the mean of this array is used as a convergence tolerance. This correction process continues iterating until the convergence tolerance is below the user specified limit.

2.2.4 Measurement uncertainty of each system

While the CPMA-DMS systems have many advantages, such as the ability to measure transient mass-mobility sources or entire density distributions from steady state sources in minutes, these characteristics come at the cost of uncertainty. Using a 95% confidence interval, a CPMA has a 2.8% uncertainty in mass-to-charge setpoint (Symonds et al., 2013), while a DMA has a 3% uncertainty in mobility size (Mulholland et al., 1999). Therefore through propagation of uncertainty, a DMA-CPMA system has a 9.4% uncertainty in effective density. Symonds (2010), also using a 95% confidence interval, found the uncertainty in a standard DMS is 10% in mobility size. Therefore, the effective density uncertainty in the CPMA-sDMS system is 30.1%. The uncertainty in the modified DMS was determined by finding the uncertainty in the size calibration fit using the least-squares regression analysis outlined by Figliola and Beasley (2010). Propagating the fit uncertainty with the DMA bias uncertainty, the modified DMS mobility size uncertainty was determined to be between 3.04–3.35% depending on particle mobility size. Therefore through propagation of error, the CPMA-mDMS system has an effective density uncertainty of 9.5–10.4% depending on particle mobility size.

2.3 Results and discussion

The experimental set-up and correction method was validated by measuring the effective density of DEHS with two neutralizer-CPMA-DMS systems. DEHS was chosen as its droplets have a spherical morphology and its density remains constant over a range of mobility sizes. The accepted effective density was determined from Haynes (2013) to be 912 kg/m^3 at the DMS classifier conditions (T=298 K).

2.3.1 Size calibration

Accurate particle sizing is extremely important for mass-mobility measurements as effective density is proportional to the particle mobility diameter cubed. A 5% measurement error in particle sizing results in a 15% error in measured effective

density.[2] To limit the uncertainty in sizing both the standard and modified DMS were calibrated.

The modified DMS was calibrated with a DMA by atomizing the aerosol material, classifying it with a DMA, and then measuring the DMA-classified aerosol with the modified DMS as shown in Figure 2-5. The effects of multiple-charging from the DMA did not affect the calibration as both the DMA and modified DMS size particles by electrical mobility. Therefore, after size selection by the DMA, a multiply-charged particle would have the same electrical mobility as a singly-charged particle and would be detected on the same ring as a singly-charged particle in the modified DMS.

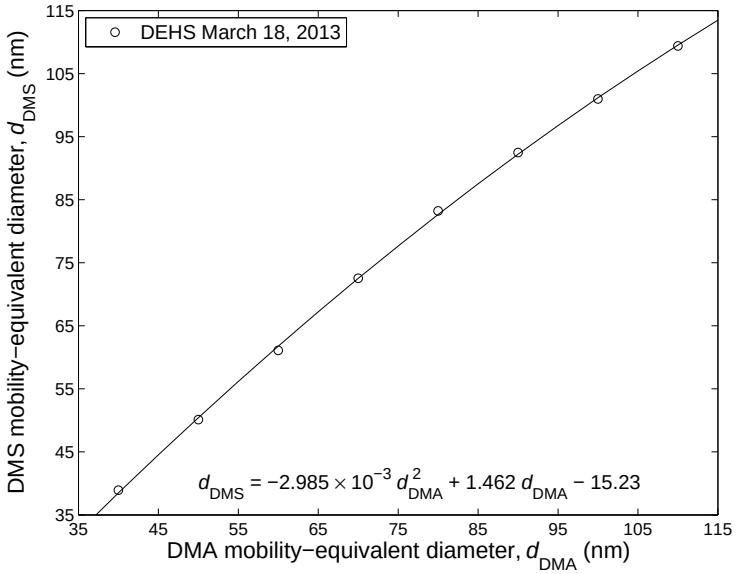

Figure 2-5: Mobility size calibration curve of modified DMS with DEHS particles.

The calibration curve for the standard DMS is shown in Figure 2-6 using DEHS and polystyrene latex spheres (PSL). Multiple-charging effects from the DMA affect the standard DMS as the aerosol is re-charged between the DMA outlet and DMS column inlet, changing the electrical mobility of the particles, and introducing a small error in the calibration (determined to be approximately 2.85%). Therefore, the standard DMS was also calibrated with PSL (a monodispersed aerosol), and

[2] From Eq. 1.2, $\frac{u_{\rho_{\text{eff}}}}{\rho_{\text{eff}}} = \sqrt{\left(\frac{u_m}{m}\right)^2 + 9\left(\frac{u_{d_\text{m}}}{d_\text{m}}\right)^2}$, where u is the uncertainty.

the DMA was not used. Even though the standard DMS calibration using DEHS and a DMA was affected by multiply-charging, the data was still included in the calibration curve. This data was used because calibration with PSL below 200 nm is difficult to complete due to interference from smaller particles caused by impurities in the PSL-water suspension.

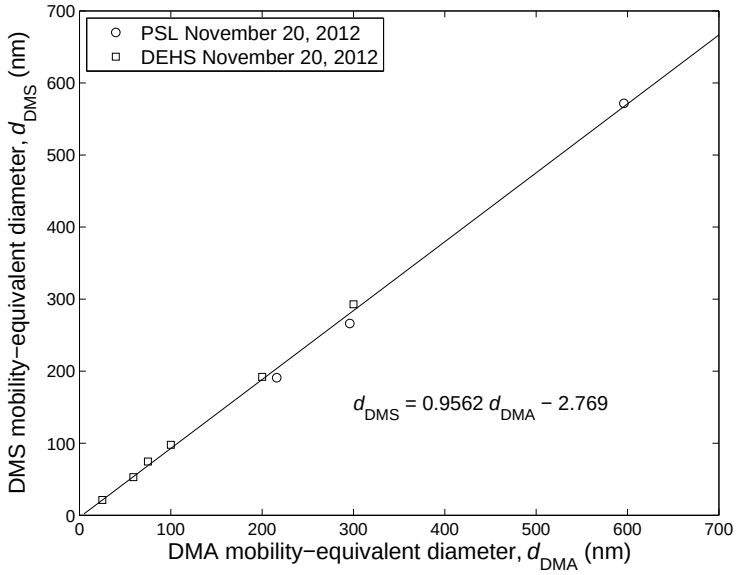

Figure 2-6: Mobility size calibration curve of standard DMS with PSL and DEHS particles.

2.3.2 CPMA - modified DMS results

The effective density of DEHS measured by the CPMA-mDMS system, at a CPMA resolution of 3 and using the Wiedensohler bipolar charging model within the correction process, is shown in Figure 2-7a. The average measured effective density was 964 kg/m^3 or within 5.7% of the accepted value. The error bars represent the instrument bias uncertainty of 9.5–10.4% depending on particle mobility size as previously determined. Applying a 95% confidence interval the precision uncertainty of the CPMA-mDMS was 33 kg/m^3 and the total uncertainty was 89 to 115 kg/m^3 (10.3 to 10.9%) depending on the particle mobility size.

The multiple-charge correction and size calibration changed the effective density by a maximum of -29.2% compared to the uncorrected effective density (calculated

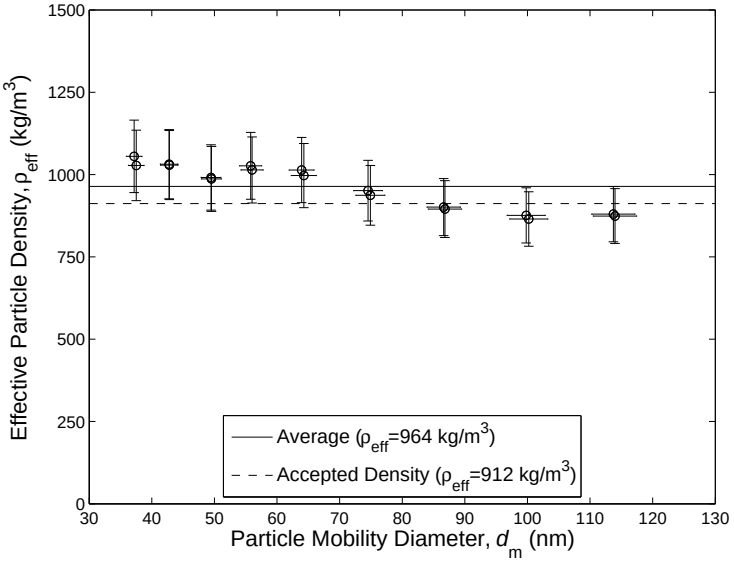

(a)

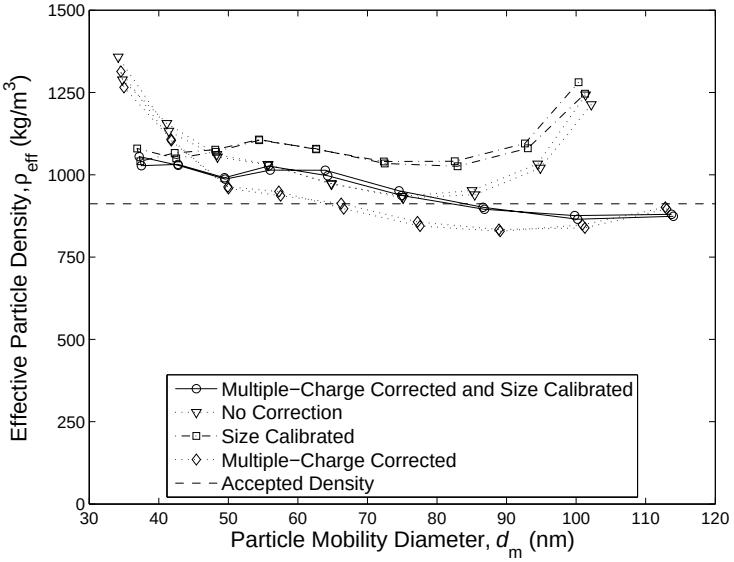

(b)

Figure 2-7: (a) Measured effective density of DEHS using a CPMA, with a resolution of 3, and modified DMS system, applying the Wiedensohler bipolar charging model within the correction process. (b) Comparison of DEHS effective density values calculated from the data described in (a) with: (i) no correction, (ii) size calibration only, (iii) multiple-charge correction only and (iv) multiple-charge correction and size calibration.

from the uncorrected mDMS CMD). The magnitude of each correction is shown in Figure 2-7b. The size calibration (shown previously) showed the modified DMS over-sized the particles from 50-100 nm and under-sized the particles otherwise. Therefore the size calibration either increased or decreased the measured effective density depending on the particle mobility size. However, the multiple-charge correction removed current from the lower DMS ring numbers (or smaller particle sizes), making the corrected CMD higher and the effective density lower over the entire mobility range. Compared to the uncorrected effective density, the size calibration caused a maximum change in effective density of -20.5%, while the multiple-charge correction caused a maximum change in effective density of -27.5%. Therefore, both the multiple-charge correction and size calibration are required to accurately operate a CPMA-mDMS system.

Effects of bipolar charging model on CPMA-mDMS system

The Gopalakrishnan et al. bipolar charging model was also applied within the correction process, rather than Wiedensohler's model, to estimate the effect of the bipolar charging model on the data inversion. This variation of the correction process, applied to the same data described above, calculated an average DEHS effective density of 997 kg/m^3 or within 9.3% of the accepted value. This value is still within error of the accepted value and is within 3.4% of the average effective density generated using the Wiedensohler model. The results of this comparison, using a CPMA resolution of 3, are shown in Figure 2-8.

The Gopalakrishnan et al. bipolar model was implemented assuming that the DEHS particles were spherical (liquid) and nonconducting (electric resistivity of DEHS is 6.9×10^{11} ohm·cm) (Karzhev et al., 1969).

Effects of CPMA resolution on CPMA-mDMS system

DEHS results were also collected using a CPMA resolution of 5 to estimate the effect of different CPMA resolutions on the data inversion. These data measured an average DEHS effective density of 979 kg/m^3 or within 7.3% of the accepted value.

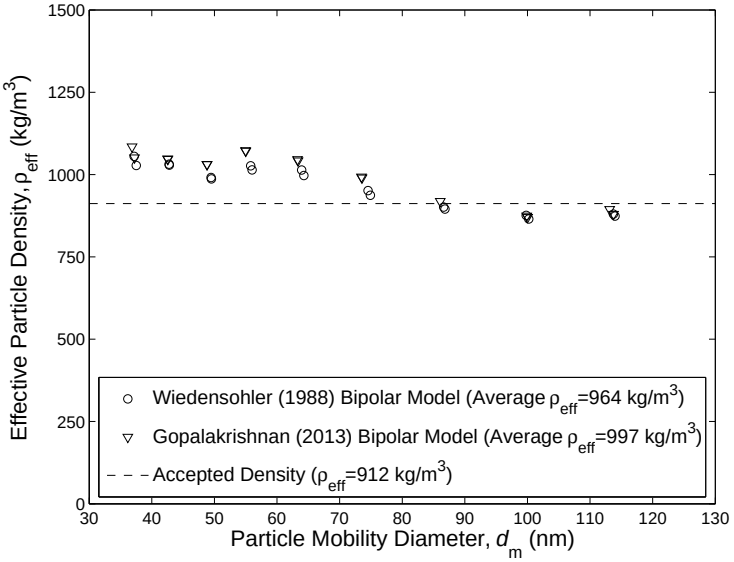

Figure 2-8: Effects of the bipolar charging model on the DEHS effective density results measured using the CPMA-mDMS system with a CPMA resolution of 3.

This value is also within error of the accepted value and is within 1.5% of the average effective density measured using a CPMA resolution of 3. A plot comparing these results is shown in Figure 2-9 and demonstrates that a range of CPMA resolutions can be used within the CPMA-mDMS system.

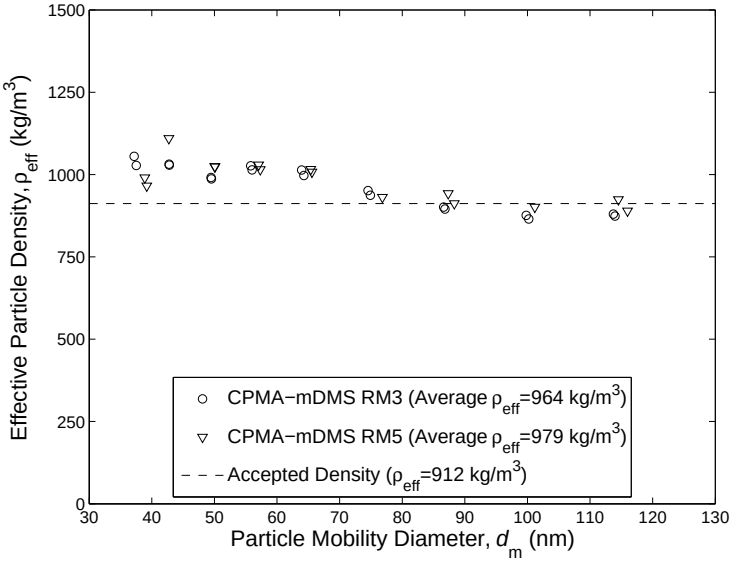

Figure 2-9: Effects of CPMA resolution on the DEHS effective density results measured using the CPMA-mDMS system and applying Wiedensohler's bipolar charging model within the correction process.

2.3.3 CPMA - standard DMS results

The effective density measured by the CPMA-sDMS system is shown in Figure 2-10a. The CPMA resolution was 10. The full charging model was used (DMS model 1), which considers the entire charge distribution for each particle mobility size leaving the DMS corona charger. The Wiedensohler bipolar and Fuchs unipolar charging models were applied within the correction process and the DMS ring currents generated by uncharged particles that pass through the CPMA were manually removed (Method I). The averaged measured effective density was 1027 kg/m^3 or within 12.6% of the accepted value. The error bars represent the instrument bias uncertainty of 30.1% as previously determined. Applying a 95% confidence interval the precision uncertainty of the CPMA-sDMS was 41 kg/m^3 or 4.5% of the accepted value, which is insignificant compared to the bias uncertainty of 30.1%. Therefore the total uncertainty in the measured effective density is approximately 30.1%. Figure 2-10a also shows the presence of a systematic error with a nearly constant offset from the accepted value.

The multiple-charge correction and size calibration changed the effective density by a maximum of -13.3% compared to the uncorrected effective density (calculated from the uncorrected sDMS CMD). The magnitude of this correction is misleading, as the multiple-charge correction and size calibration were counteracting each other, as shown Figure 2-10b. The standard DMS size calibration makes the corrected CMD higher (and the effective density lower), while the multiple-charge correction removed current from the upper DMS ring numbers (or larger particle sizes), making the corrected CMD lower (and the effective density higher). Compared to the uncorrected effective density, the size calibration caused a maximum change in effective density of -23.3%, while the multiple-charge correction caused a maximum change in effective density of +28.4%. Therefore, both the multiple-charge correction and size calibration are not small enough to neglect and are required to accurately operate a CPMA-sDMS system.

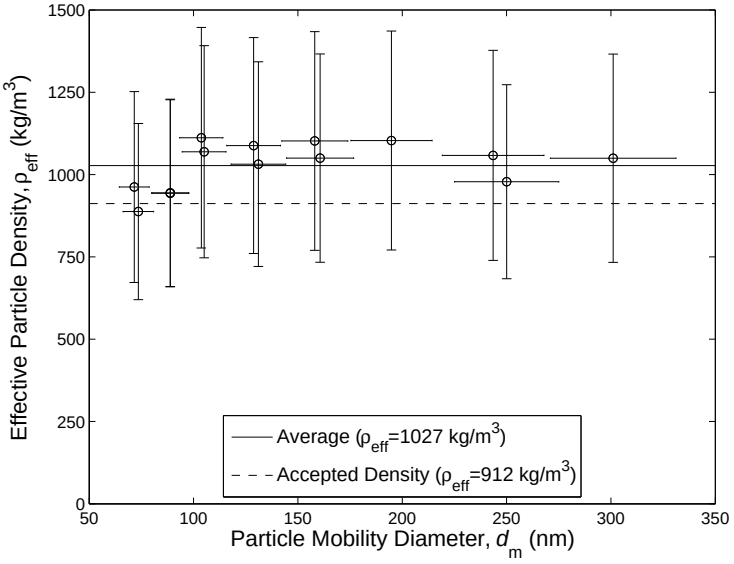

(a)

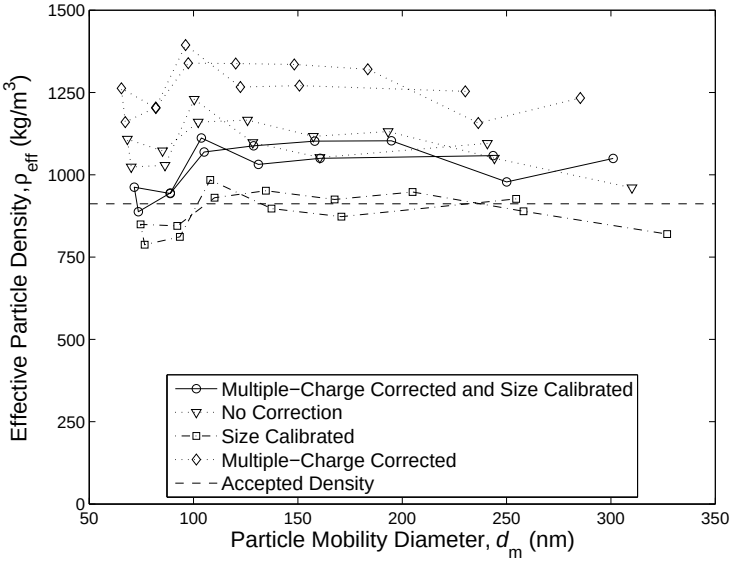

(b)

Figure 2-10: (a) Measured effective density of DEHS using CPMA, with a resolution of 10, and standard DMS system, applying the Wiedensohler bipolar and Fuchs unipolar charging models within the correction process. (b) Comparison of DEHS effective density values calculated from the data described in (a) with: (i) no correction, (ii) size calibration only, (iii) multiple-charge correction only and (iv) multiple-charge correction and size calibration.

Effects of unipolar charging model on CPMA-sDMS system

The White unipolar charging model was also applied within the correction process, rather than Fuchs' model, to estimate the effect of the unipolar charging model on the data inversion. This variation of the correction process, applied to the same data described above, calculated an average DEHS effective density of 1033 kg/m^3 or within 13.3% of the accepted value. This value is still within error of the accepted value and is within 0.6% of the average effective density generated using the Fuchs model. The results of this comparison, using a CPMA resolution of 10 and applying Wiedensohler's bipolar charging model within the correction process, are shown in Figure 2-11.

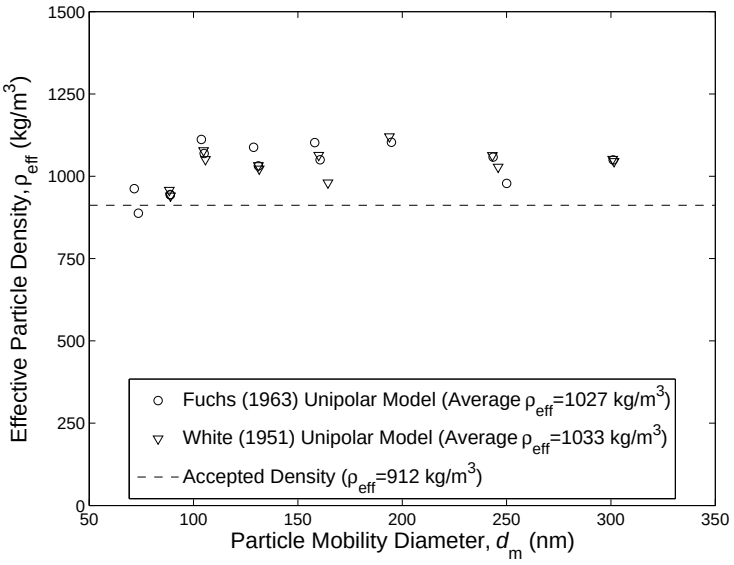

Figure 2-11: Effects of the unipolar charging model on the DEHS effective density results measured using the CPMA-sDMS system with a CPMA resolution of 10 and applying Wiedensohler's bipolar charging model within the correction process.

The Fuchs unipolar model was implemented assuming that the DEHS particles have a dielectric constant of 3.7 (Karzhev et al., 1969).

Effects of CPMA resolution on CPMA-sDMS system

DEHS results were also collected using a CPMA resolution of 5 to estimate the effect of different CPMA resolutions on the data inversion. These data measured

an average DEHS effective density of 1028 kg/m^3 or within 12.7% of the accepted value. This value is also within error of the accepted value and is within 0.05% of the average effective density measured using a CPMA resolution of 10. A plot comparing these results is shown in Figure 2-12 and demonstrates that a range of CPMA resolutions can be used within the CPMA-sDMS system.

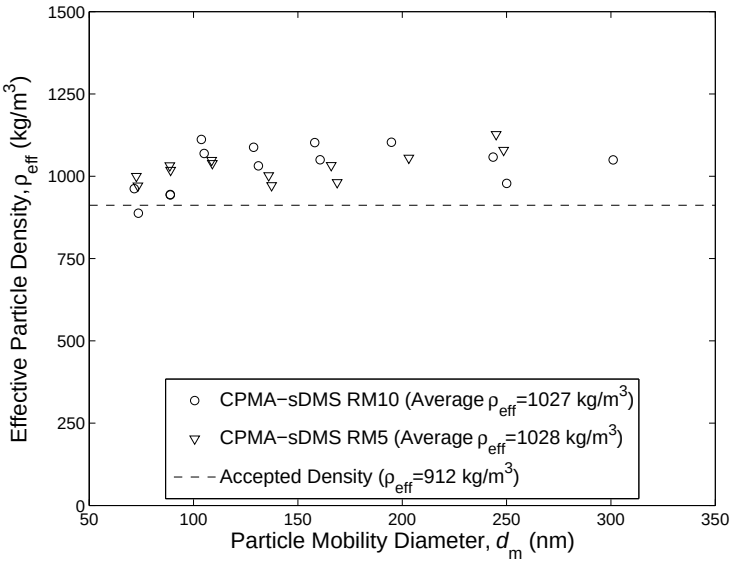

Figure 2-12: Effects of CPMA resolution on the DEHS effective density results measured using the CPMA-sDMS system and applying Wiedensohler's bipolar and Fuchs' unipolar charging models within the correction process.

Average versus full charging models

For the CPMA-sDMS system, the average charging model (DMS Model 2) only considers the mean charge for each particle mobility size leaving the DMS corona charger, rather than the entire charge distribution (DMS Model 1 or 3). DMS Model 1 applies the charge probabilities to each CPMA classified mobility size concentration, while DMS Model 3 applies the diffusive DMS model, based on the charging probabilities. The effects of these assumptions are shown in Figure 2-13 where for all of the cases the current generated by uncharged particles was manually removed, a CPMA resolution of 10 was used and Wiedensohler bipolar and Fuchs unipolar charging models were applied within the correction process. The effective densities found using the average charging model (DMS Model 2) disagreed on average by

4.3% with the values found using DMS Model 1. However, DMS Model 2 only generated 12 valid data points out of 16 inputs, where the theoretical and measured DMS ring currents agreed within a set tolerance of 5%, compared to 14 valid data points generated by DMS Model 1. The effective densities found using DMS Model 3 disagreed on average by 1.3% with the values found using DMS Model 1. DMS Model 3 generated 15 valid data points out of 16 inputs. On average the time to apply the correction per point per iteration took 526 seconds for DMS Model 1, 323 seconds for DMS Model 2, and 548 seconds for DMS Model 3. Due to the nature of Fuchs' unipolar model (solving differential equations), DMS model 3 takes longer to calculate than DMS model 1; however if White's unipolar model (which has an analytical solution) is applied instead, DMS model 3 becomes faster than DMS model 1.

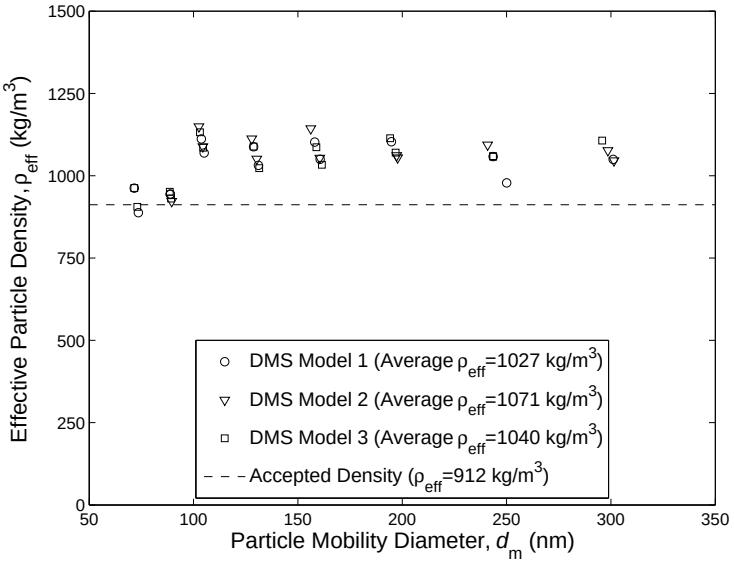

Figure 2-13: DEHS measured effective density using all three standard DMS models where the current generated by uncharged particles was manually removed for all cases, a CPMA resolution of 10 was used and Wiedensohler bipolar and Fuchs unipolar charging models were applied within the correction process.

Automatic versus manual uncharged particle removal

For the standard DMS, the effects of calculating and removing the current generated by the uncharged particles using the CPMA diffusive transfer function versus

manually removing it are shown in Figure 2-14 using DMS Model 1, a CPMA resolution of 10 and Wiedensohler bipolar and Fuchs unipolar charging models within the correction process for both cases. The effective densities found using the uncharged model disagreed on average by 1.6% with the values found by manually removing the current generated by uncharged particles. This disagreement is insignificant compared to the system uncertainty of 31%. The results that had the current generated by uncharged particles manually removed took on average 526 seconds per point per iteration to calculate, while removing the current generated by uncharged particles through the model took on average 1394 seconds per point per iteration. This large discrepancy is due to the number of points calculated in each CPMA model. The CPMA uncharged particle model calculates the transfer function at each particle mass in the mobility range (approximately 500 points); however the CPMA charged particle model calculates the transfer function in steps that are centered about the CPMA mass-to-charge setpoint (approximately 200 points). Therefore to decrease computation time, the current generated by uncharged particles can be manually removed. However, the uncharged particle model should still be used when the current generated by the uncharged particles versus the classified particles is indistinguishable (i.e. measured on common DMS rings).

Bibliography

Cambustion (2011). *DMS500 Fast Particulate Spectrometer with Heated Sample Line High Ratio Diluter User Manual*, 3.5 edition.

Figliola, R. S. and Beasley, D. E. (2010). *Theory and Design for Mechanical Measurements*. John Wiley & Sons, Inc., 5th edition.

Fuchs, N. (1963). On the stationary charge distribution on aerosol particles in a bipolar ionic atmosphere. *Geofisica pura e applicata*, 56(1):185–193.

Gopalakrishnan, R., Meredith, M. J., Larriba-Andaluz, C., and Jr., C. J. H. (2013). Brownian dynamics determination of the bipolar steady state charge distribution

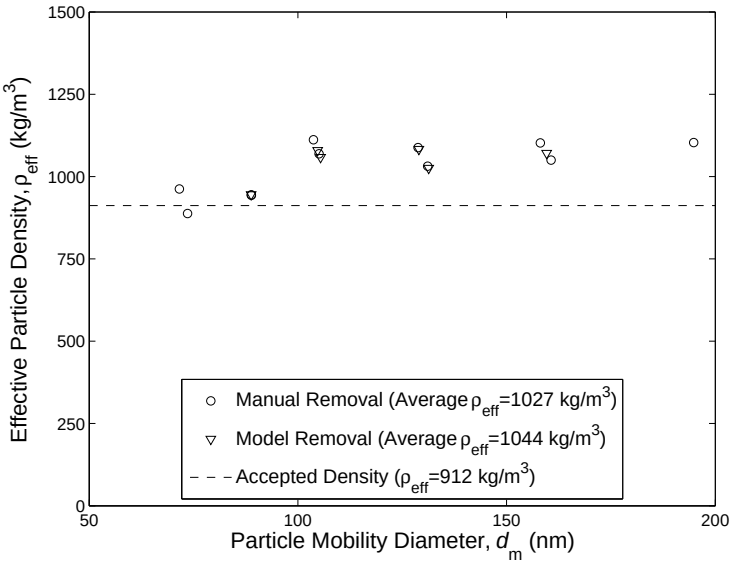

Figure 2-14: DEHS measured effective density found by manually and automatically removing the current generated by uncharged particles in the standard DMS system (using DMS model 1 for both cases).

on spheres and non-spheres in the transition regime. *Journal of Aerosol Science*, 63(0):126 – 145.

Gunn, R. and Woessner, R. (1956). Measurements of the systematic electrification of aerosols. *Journal of Colloid Science*, 11(3):254 – 259.

Haynes, W. M., editor (2012-2013). *CRC Handbook of Chemistry and Physics*. CRC Press/Taylor and Francis, Boca Raton, FL, 93rd edition. Internet Version 2013 (Accessed May 29, 2013).

Johnson, T. J., Symonds, J. P., and Olfert, J. S. (2013). Mass-mobility measurements using a centrifugal particle mass analyzer and differential mobility spectrometer. *Aerosol Science and Technology*, 47(11):1215–1225.

Karzhev, V. I., Kumleva, L. A., Makeeva, E. D., Goncharova, N. V., Sil'chenko, E. I., and Abakumova, G. S. (1969). Physical properties of alkylarylsuccinic diesters. *Khimicheskaya Promyshlennost*, 45:32–33.

Mulholland, G., Bryner, N., and Croarkin, C. (1999). Measurement of the 100 nm

NIST SRM 1963 by differential mobility analysis. *Aerosol Science and Technology*, 31(1):39–55.

Olfert, J. and Collings, N. (2005). New method for particle mass classification - the Couette centrifugal particle mass analyzer. *Journal of Aerosol Science*, 36(11):1338–1352.

Symonds, J. P. R. (2010). *Calibration of fast response differential mobility spectrometers*. Metrology of Airborne Nanoparticles, Standardisation and Applications (MANSA), National Physical Laboratory (NPL), London, UK, June 8-9, 2010.

Symonds, J. P. R. and Reavell, K. (2007). *Calibration of a Differential Mobility Spectrometer*. European Aerosol Conference, Salzburg, Austria, September 9-14, 2007.

Symonds, J. P. R., Reavell, K. S., and Olfert, J. S. (2013). The cpma-electrometer system- a suspended particle mass concentration standard. *Aerosol Science and Technology*, 47(8):i–iv.

White, H. J. (1951). Particle charging in electrostatic precipitation. *American Institute of Electrical Engineers, Transactions of the*, 70(2):1186 –1191.

Wiedensohler, A. (1988). An approximation of the bipolar charge distribution for particles in the submicron size range. *Journal of Aerosol Science*, 19:387–389.

Chapter 3

Effective density and mass-mobility exponent of aircraft particulate matter

3.1 Experimental set-up

The SAMPLE III campaign was completed at the SR Technics turbine engine test facility in Zurich, Switzerland from April 23rd to May 4th 2012. The campaign was carried out by a collaboration of international researchers and involved several simultaneous tests, where measurements were taken from turbine engines undergoing performance certification tests after being serviced. Three days of dedicated turbine engine testing, where the engine test conditions were set by the researchers, were also completed from April 28th to 30th 2012.

3.1.1 Sampling aircraft turbine engine exhaust

The experimental set-up used to collect, condition and transport the aircraft turbine exhaust to the measurement systems is shown in Figure 3-1.

Table 3-1 outlines the components, materials and dimensions of the sampling

A version or portion of this chapter has been submitted for publication/accepted for publication/published. Submitted: Johnson et al. (2013a)

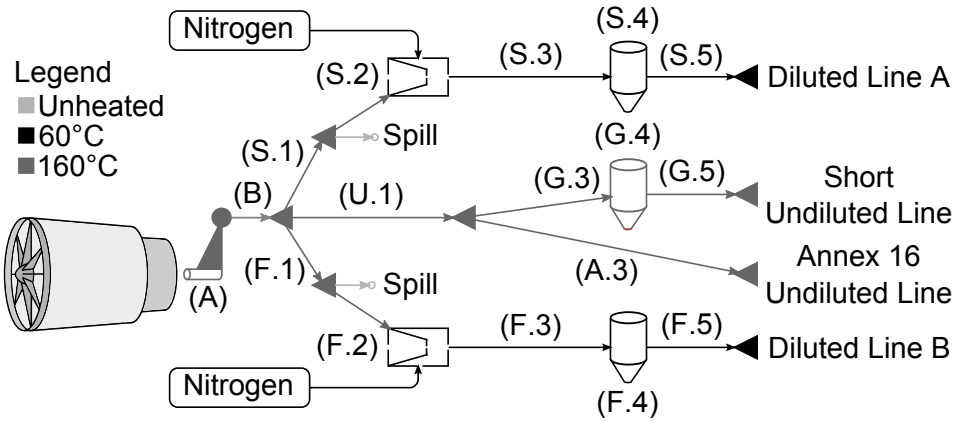

Figure 3-1: Sampling system used to collect aircraft exhaust from the exit plane of the turbine engine and transport it to the measurement systems. The sampling system consisted of the following components: (A) Sample Probe; (B) Primary Sample Line; (S.1) Diluted Primary Line A; (U.1) Undiluted Primary Line; (F.1) Diluted Primary Line B; (S.2) Primary Dilutor A; (F.2) Primary Dilutor B; (S.3) Diluted Sample Line A; (G.3) Short Undiluted Sample Line; (A.3) Annex 16 Undiluted Sample Line; (F.3) Diluted Sample Line B; (S.4) BGI Sharp-Cut Cyclone; (G.4) BGI Sharp-Cut Cyclone; (F.4) URG Stairmand Cyclone; (S.5) Diluted Secondary Line A; (G.5) Short Undiluted Secondary Line; (F.5) Diluted Secondary Line B.

system.

Table 3-1: Characteristics of experimental set-up.

Label	Component	Material	ID (mm)	OD (mm)	Length (m)	Temperature Control
(A)	Sample Probe	SS	8	10	1	Engine Exhaust Sheath Flow
(B)	Primary Sample Line	SS	8	10	6	Heat Tracing
(S.1)	Diluted Primary Line A	SS	8	10	0.34	Heat Tracing
(U.1)	Undiluted Primary Line	SS	7.75	9.525	0.34	Heat Tracing
(F.1)	Diluted Primary Line B	SS	8	10	0.34	Heat Tracing
(S.2)	Primary Dilutor A	SS	N/A	N/A	0.83	Nitrogen Heater and Heat Tracing
(F.2)	Primary Dilutor B	SS	N/A	N/A	0.8	Nitrogen Heater and Heating Bag
(S.3)	Diluted Sample Line A	PTFE	7.75	9.525	25	Stainless Steel Braid Electric Heating
(G.3)	Short Undiluted Sample Line	SS	7.75	9.525	1.4	Spiral wound Heat Tracing
(A.3)	Annex 16 Undiluted Sample Line	PTFE	6	8	12	Spiral Wound Heat Tracing
(F.3)	Diluted Sample Line B	PTFE	8	10	24.5	Spiral Wound Heat Tracing
(S.4)	BGI Sharp-Cut Cyclone	SS	N/A	N/A	N/A	Heat Tracing
(G.4)	BGI Sharp-Cut Cyclone	SS	N/A	N/A	N/A	Heating Bag
(F.4)	URG Stairmand Cyclone	SS	N/A	N/A	N/A	Heat Tracing (from F.5 bag)
(S.5)	Diluted Secondary Line A	SS	7.75	9.525	0.28	Heat Tracing
(G.5)	Short Undiluted Secondary Line	SS	7.75	9.525	0*	Heat Tracing
(F.5)	Diluted Secondary Line B	SS	7.75	9.525	0.28	Heating Bag

PTFE= Carbon Loaded or Conductive PTFE SS=Stainless Steel *0 m to DMS, 0.2 m to LII

The sample was collected using a probe placed at the center line of the engine. The probe was transversable in the vertical plane and was maintained at a tempera-

ture above 160°C using a 25 mm coaxial sleeve that forced hot exhaust flow around the probe. All components downstream of the probe were maintained at the shown temperatures using some form of electrical heating such as heat tracing or heating bags to avoid the condensation of volatile material or water and particle losses due to thermophoresis.

Four different samples lines were used to measure the effects of various sampling parameters, such as line length and temperature on the results. Diluted Lines A and B both diluted the sample with nitrogen by a 10(±2):1 ratio using a Dekati Di-1000 eductor diluter and a nitrogen heater (DH-1723, Dekati). These diluted lines (DL) were identical in every aspect, except for the primary splitter and main sample line characteristics. Diluted Line A had a 1 inch three-way splitter (S.1) and the main sample line (S.3) was 25 m long with a 7.75 mm ID and 9.525 mm OD. Diluted Line B had an 8 mm three-way splitter (F.1) and the main sample line (F.3) was 24.5 m long with an 8 mm ID and 10 mm OD. These differences were assumed to be negligible when generating the effective density results. The Short Undiluted Line was used to measure the sample as close as possible to the engine exhaust outlet, while the Annex 16 Undiluted Line was used to measure the gas phase emissions. Both of these undiluted lines (UL) only conditioned the sample through line heating. The total length of the Annex 16 Undiluted Line and Short Undiluted Line were 13.8 m and 24.4 m shorter than Diluted Line A respectively.

The placement of the aerosol characterization instruments on each sample line when the CPMA-mDMS system was used is shown in Figure 3-2.

Table 3-2 outlines the instruments used to characterize the aircraft particulate matter.

The CPMA-mDMS system measured the exhaust from a CFM56-5B4-2P turbine engine on April 29th and April 30th, a CFM56-7B26-3 turbine engine on May 2nd and a PW4000-100 turbine engine on May 3rd. The arrangement of the instruments changed from day to day to test the effects of different sampling parameters such as the sample line temperature and length on the results. Further details about the sampling system and the results comparing the sampling parameters are described

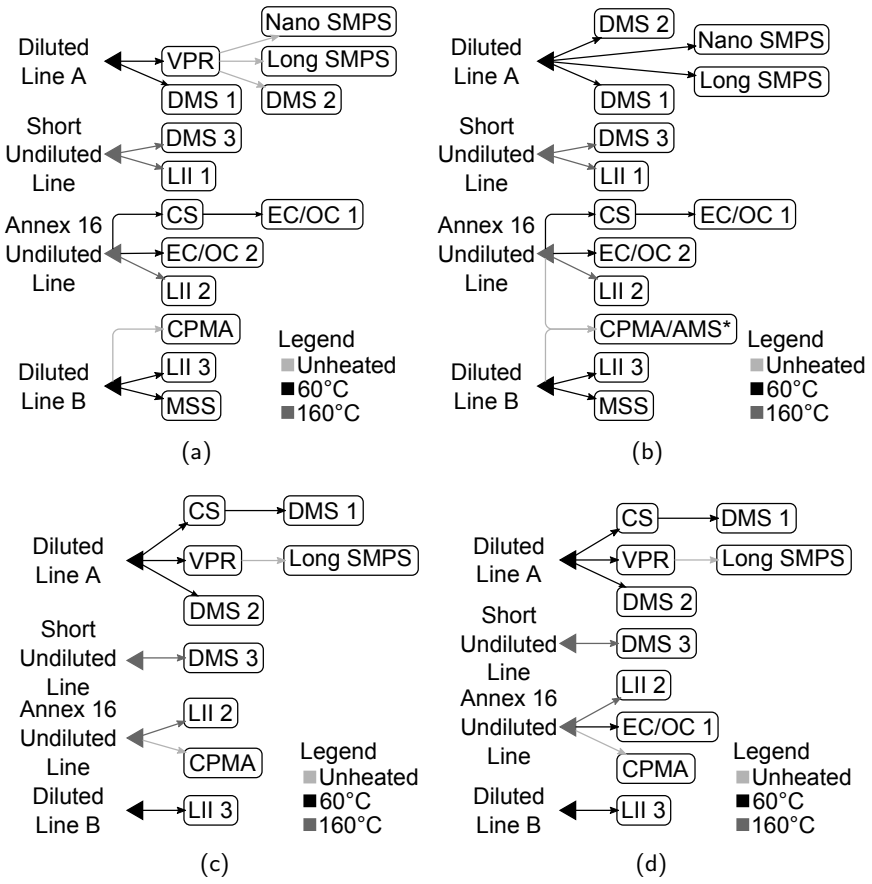

Figure 3-2: Experimental set-ups used for: (a) CFM56-5B4-2P turbine engine on April 29th 2012; (b) CFM56-5B4-2P turbine engine on April 30th 2012; (c) CFM56-7B26-3 turbine engine on May 2rd 2012; (d) PW4000-100 turbine engine on May 3rd 2012.

Table 3-2: Characteristics of aerosol instruments.

Label	Instrument	Manufacturer	Measurement	Variable	Units
CPMA	Centrifugal Particle Mass Analyzer	Cambustion	Particle Mass	m_p	fg
DMS	Differential Mobility Spectrometer 500	Cambustion	Particle mobility size distribution	$dN/d\log d_m$	cm^{-3}
Long SMPS	Long Scanning Mobility Particle Sizer	TSI	Particle mobility size distribution	$dN/d\log d_m$	cm^{-3}
Nano SMPS	Nano Scanning Mobility Particle Sizer	TSI	Particle mobility size distribution	$dN/d\log d_m$	cm^{-3}
LII	Laser Induced Incandescence	Artium	nvPM Mass Concentration	M	ug/m^3
MSS	Micro Soot Sensor	AVL	nvPM mass concentration	M	ug/m^3
EC/OC	Elemental and Organic Carbon Filters	-	PM mass concentration	M	ug/m^3
CS	Catalytic Stripper	-	Removes volatile components of PM by heating	N/A	N/A
VPR	Volatile Particle Remover	AVL	Removes volatile components of PM by heating and dilution	N/A	N/A

by Crayford et al. (2012).

3.1.2 CPMA-mDMS system

The experimental set-up of the CPMA-mDMS system is shown in Figure 3-3. This set-up was used rather than a differential mobility analyzer (DMA), CPMA and condensation particle counter (CPC) system due to the short sampling time allowed at each engine load point. A CPMA-DMS system is capable of measuring an eight point effective density function in approximately the same time as a DMA-CPMA-CPC system measuring one point (Johnson et al., 2013b). This difference is due to the scanning nature of the DMA-CPMA-DMS system at each particle mobility size, that is not required in the CPMA-DMS system. However this characteristic increased the measurement uncertainty slightly, 9.5%-10.4% compared to 9.4% in terms of effective density as calculated by Johnson et al. (2013b).

Three-way valves A and B, shown in Figure 3-3, were only used on April 30th and allowed the CPMA-mDMS system to sample from either Diluted Sample Line B or the Annex 16 Undiluted Sample Line. To maintain system flow balance, the line that was not being sampled by the CPMA-mDMS system was sampled by an Aerosol Mass Spectrometer (AMS). For the other test days the sample location of the CPMA shown in Figure 3-2 was connected directly to the inlet of three-way valve C. To test the effects of particle volatility three-way valve C also allowed the sample to bypass the catalytic stripper (CS). This work refers to sample that has passed through the catalytic stripper as denuded (D) and sample that has bypassed as undenuded (UD). The catalytic stripper, which consisted of two catalyzed ceramic substrates and a sulfur trap, was heated to a 350°C. A complete description of this catalytic stripper and its effects on the sample are found in Swanson (2013) and references therein.

A radioactive neutralizer was used to charge the sample upstream of the CPMA. The CPMA classifies particles by their mass-to charge ratio (Olfert and Collings, 2005). This is accomplished by passing the sample between two concentric spinning cylinders, thus applying a centrifugal force to the particles. A voltage potential is

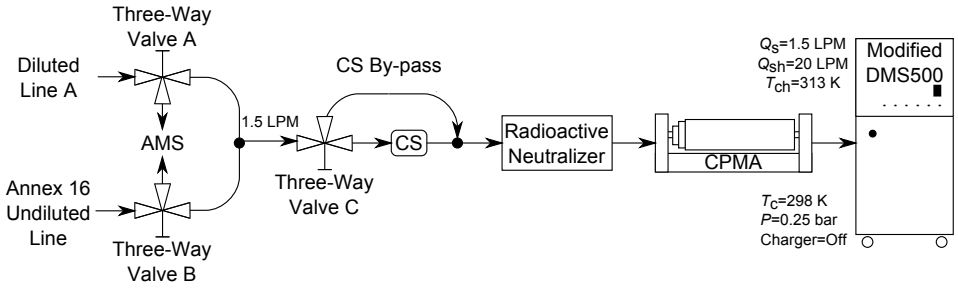

Figure 3-3: Experimental set-up of the CPMA-modified DMS system that was used to measure the mass-mobility of individual aerosol particles where: CS is a catalytic stripper, Q_{s} is the DMS classifier sample flow rate, Q_{sh} is the DMS classifier sheath flow rate, T_{ch} is the DMS charger temperature, T_{c} is the DMS classifier temperature and P is the DMS classifier pressure.

also placed across the cylinders applying an electrostatic force to the particles as well. Therefore particles of a set mass-to-charge ratio induce an equal electrostatic and centrifugal force in opposite directions and pass through the classifier. By changing the voltage and speed applied to the cylinders, the mass-to-charge setpoint can be controlled. Uncharged particles can also pass through the CPMA if they are smaller than the cut-off mass for a given rotational speed (Symonds et al., 2013).

A modified DMS500 (mDMS) was used to measure the mobility size distribution of the CPMA classified particles. The DMS500 classifies particles by their electrical mobility in real time thus measuring the transient mobility size distribution (Reavell et al., 2002; Biskos et al., 2005). A voltage potential is placed between two concentric cylinders and the path of the particles from the inside cylinder to the outside cylinder is only dependent on their electrical mobility. Twenty-two electrometer rings are placed on the inner surface of the outer cylinder and measure the current generated from these particles grounding their charges at impact. By applying an inversion to these measured currents the electrical mobility size spectral of the particles is determined.

The DMS500 unipolar charger is a significant source of uncertainty, both for particles in the range of 20-80 nm (in the region where doubly-charged particles start to occur), and due to morphological sensitivity of the charging process (Symonds and Reavell, 2007; Symonds, 2010), compared with its classifier alone. Therefore the

charger was disabled and the DMS500 was run just as a particle mobility classifier, relying on the pre-existing charge from the neutralised and CPMA classified aerosol, to improve the sizing accuracy and remove most of the morphological dependence from the measurement. As a result, the particles had lower charge states and thus lower electrical mobilities and required a longer residence time within the DMS to be classified. This was achieved by dropping the sheath flow rate from 30 slpm to 20 slpm and the sample flow rate from 8 slpm to 1.5 slpm. These modifications limited the sizing range of the mDMS from 10 nm to 120 nm. The inversion matrix applied to the mDMS assumed all particles were singly charged and generated 64 size-classes per decade. Two additional benefits of these modifications were the lower sample flow rate of 1.5 slpm allowed the CPMA to operate at higher resolutions at lower speeds and the mDMS measurements were not affected by small uncharged particles that pass through the CPMA, as the particles were not detected on the mDMS electrometer rings.

Since the CPMA classified particles by their mass-to-charge ratio and multiply-charged particles were present, the mDMS measured the mobility size distribution of several different particle masses. Therefore the results had to be corrected for this effect. This correction was accomplished by measuring the aerosol size distribution independently[1], using either an SMPS or DMS. The charge distribution of the neutralized aerosol was approximated using the bipolar charging model developed by Wiedensohler (1988), then the theoretical CPMA and DMS transfer functions were applied to this distribution, determining the theoretical DMS ring currents generated. The difference between the experimental and theoretical DMS ring currents was minimized using three scaling factors. After minimization the fraction of DMS ring current generated by multiply-charged particles was removed and the corrected currents were reinverted to determine the corrected DMS mobility size distribution. This distribution was fitted with a lognormal function and the fitted count median

[1]For some cases the unclassified mobility size distribution was approximated from a distribution measured on a different sample line by accounting for the different dilution ratios measured using gas analyzers and using a model developed by Liscinsky and Hollick (2010) to approximate the differences in the particle losses between the two lines.

diameter (CMD) was corrected with the size calibration curve. By combining the multiply-charge corrected and size calibrated CMD and the CMPA mass-to-charge setpoint the average effective density of that setpoint was determined. Further details of the CPMA-mDMS setup, the multiple-charge correction process and its experimental validation are described by Johnson et al. (2013b). The uncertainty of the CPMA-mDMS system was 3.04-3.35% in terms of mobility size and 9.5-10.4% in terms of effective density depending on the particle mobility size (Johnson et al., 2013b). These uncertainties apply to all of the effective density results shown in this chapter.

3.2 Results and discussion

3.2.1 Size calibration

The modified DMS (mDMS) was calibrated by using a differential mobility analyzer (DMA) to size select aerosol particles, based on their mobility, upstream of the mDMS. Multiple charging effects of the DMA did not affect the calibration as the aerosol is not recharged between the DMA outlet and DMS classifier as in a standard DMS500. Therefore a singly-charged particle selected by the DMA will land on the same DMS ring as a multiply-charged particle selected by the DMA as both particles have the same electrical mobility. Figure 3-4 shows the size calibration of the modified DMS was stable over almost a year period and for a variety of aerosols.

3.2.2 Effective density functions

The effective particle densities measured from the CFM56-5B4-2P turbine engine on April 29th and 30th at each engine load point are shown in Figure 3-5. Typical of combustion sources, the effective density decreased as mobility size increased indicating the particles were probably fractal-like aggregates. The mass-mobility exponent, as defined by Equation 1.2, varied between 2.72 and 2.82 for all engine loads and different sample conditioning. A few mass-mobility exponents did fall outside this range. This occurred for effective density functions where only a few

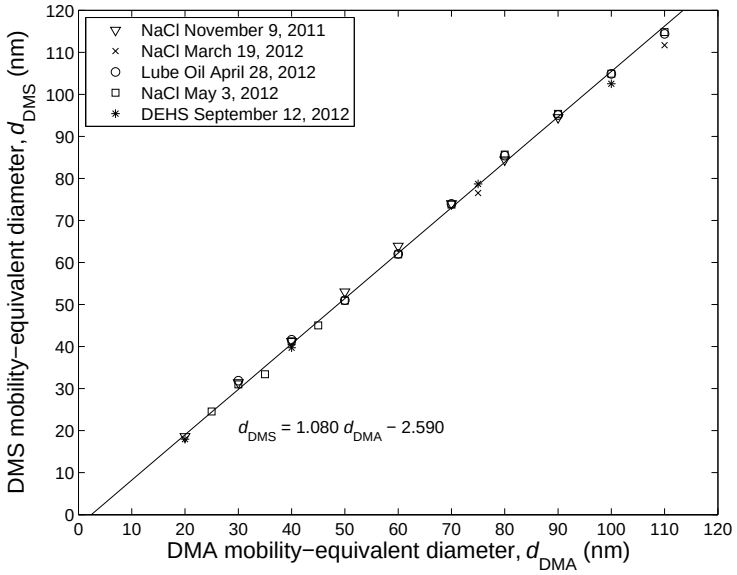

Figure 3-4: Size calibration curve of modified DMS.

points were measured across a narrow portion of the mobility size distribution due to insufficient mDMS signal from low particle concentrations, as shown in Figure 3-5e Diluted Line B, Denuded and Annex 16 Undiluted Line, Denuded. Other discrepancies were due to a maximum effective density that appeared in the middle of the effective density function. This usually occurred in the Annex 16 Undiluted Line, Undenuded, as shown in Figure 3-5c and Figure 3-5e. One possible explanation for this peak is the CPMA classified multiple species of varying effective densities as the undiluted, undenuded line had the highest possibility of delivering a multi-species sample. This peak also appeared in Figure 3-5a Diluted Line B, Denuded; however, this isolated peak was only generated by the smallest mobility size effective density decreasing. If this point is considered an outlier the remaining effective density function followed a fractal-like relationship.

These high mass-mobility exponents also indicate that the particles from turbine engines are slightly more compact or spherical than particles produced from other combustion sources such as diesel engines. Olfert et al. (2007) measured mass-mobility exponents of 2.22 to 2.48 at low diesel engine load points, while Park et al. (2004b) measured a diesel engine mass-mobility exponent of 2.35. Further analysis of this CPMA-mDMS data regarding turbine engine particle morphology and results

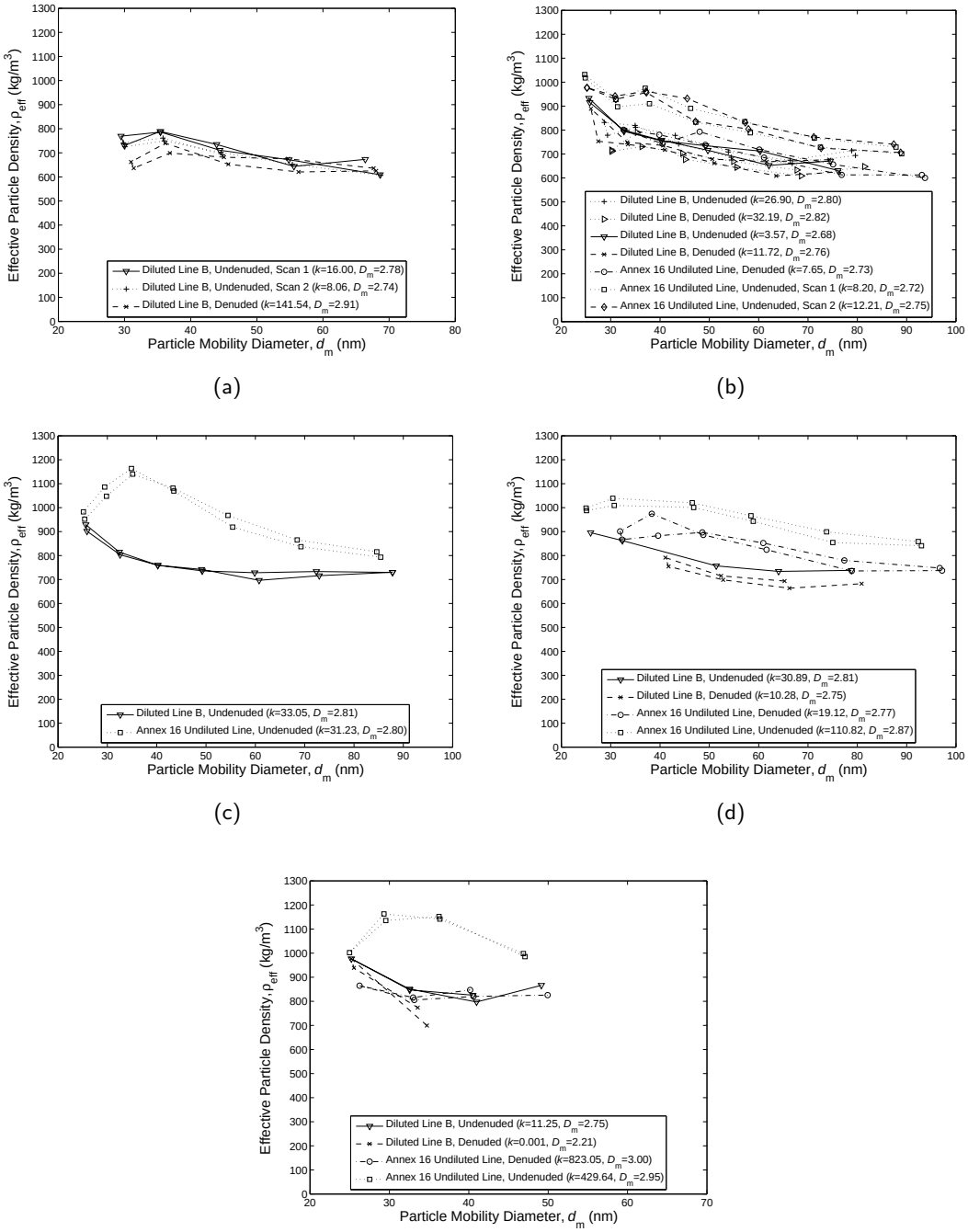

Figure 3-5: Effective density results from CFM56-5B4-2P turbine engine where the engine thrust was approximately steady-state with an average of: (a) 2560 lbs; (b) 4690 lbs; (c) 5850 lbs; (d) 6590 lbs; (e) 8330 lbs.

from other instruments at the SAMPLE III campaign, such as Transmission Electron Microscopy (TEM) images, has been completed by Boies (2013).

At the same particle mobility sizes across all engine load points, Diluted Line B had on average a 35.5 kg/m^3 lower effective density than the Annex 16 Undiluted Line for a denuded sample and a 149.4 kg/m^3 lower effective density for an undenuded sample. Similarly, the denuded sample had on average a 45.8 kg/m^3 lower effective density than the undenuded sample from Diluted Line B and a 191.4 kg/m^3 lower effective density from the Annex 16 Undiluted Line. These shifts in the effective density functions indicate the presence of volatile material within the sample. As expected the shift between the denuded and undenuded sample was smaller in the diluted line than the undiluted line, as the dilution lowered the volatile material partial vapor pressure in the line, making it less likely for volatile material to condense. The presence of volatile material in aircraft exhaust has been observed in other studies, such as Anderson et al. (1998), Dakhel et al. (2007) and Peck et al. (2012). Therefore a volatile component remover, such as a catalytic stripper, volatile particle remover (VPR) or thermodenuder, must be used to denude the volatile fraction if future regulations require the measurement (mass or number concentration) of only the non-volatile particulate matter. For further details regarding aircraft particle volatility please see Swanson (2013), which outlines the particle volatility measured during the SAMPLE III campaign using CPMA-mDMS, EC/OC filters and aerosol mass spectrometer (AMS) data.

Volatile material usually has a lower density than non-volatile material (assumed to be black carbon), approximately 1000 kg/m^3 vs. 1800 kg/m^3 (Park et al., 2004a) respectively. As the portion of volatile material increases the effective particle density will also increase until the particle becomes spherical. This effect is due to the fractal-like nature of a soot particle, where the volatile material fills in the voids around the primary soot particles, thus increasing the particle mass significantly, while only causing a small increase in the particle mobility diameter. This theory is supported by the values above as the measured effective density, at the same mobility size, increased when more volatile material was likely present.

The variations in effective density functions due to engine thrust for each sample conditioning is shown in Figure 3-6. With the exception of Figure 3-6a, all of the plots in Figure 3-6 show that the effective density increased as engine thrust increased. Figure 3-6a illustrates that the effective density initially increased as engine thrust increased, then decreased for higher engine thrust. Timko et al. (2010) found that the average effective density, measured using an AMS and SMPS, increased slightly as engine thrust increased. However using a MAAP and SMPS, which measures a different definition of effective density than the AMS and SMPS, Timko et al. (2010) found that this average effective density initially increased as engine thrust increased then decreased at higher engine thrust. The CPMA-mDMS results can be compared against Timko et al.'s second measurement of effective density as both methods are based on particle mass and mobility diameter. Using the MAAP and SMPS, Timko et al. (2010) measured a mass-weighted average effective density of 710 kg/m^3 to 840kg/m^3, which falls within the range of the size-resolved effective densities measured by the CPMA-mDMS system of approximately 600 kg/m^3 to 1200 kg/m^3.

To determine the change in effective density due to engine thrust, yet account for the effective density being a function of particle mobility size, the standard error of fit as defined by Figliola and Beasley (2010) was determined for each sampling condition. This parameter is a measure of the spread or deviation of the data about the line of best fit. The denuded and undenuded samples on Diluted Line B had standard errors of fit of 55.1 kg/m^3 and 53.1 kg/m^3 respectively, while the denuded and undenuded samples on the Annex 16 Undiluted Line had standard errors of fit of 69.2 kg/m^3 and 99.5 kg/m^3 respectively. Therefore, engine thrust had the smallest effect on the diluted line (Figure 3-6b and 3-6c) and the largest effect on the undiluted, undenuded line (Figure 3-6b) as depicted by the spread of the effective density in each plot at common mobility sizes. These trends could indicate the non-volatile particle effective density is less sensitive to engine thrust than the total effective density or that the amount of volatile material present is dependent on engine thrust.

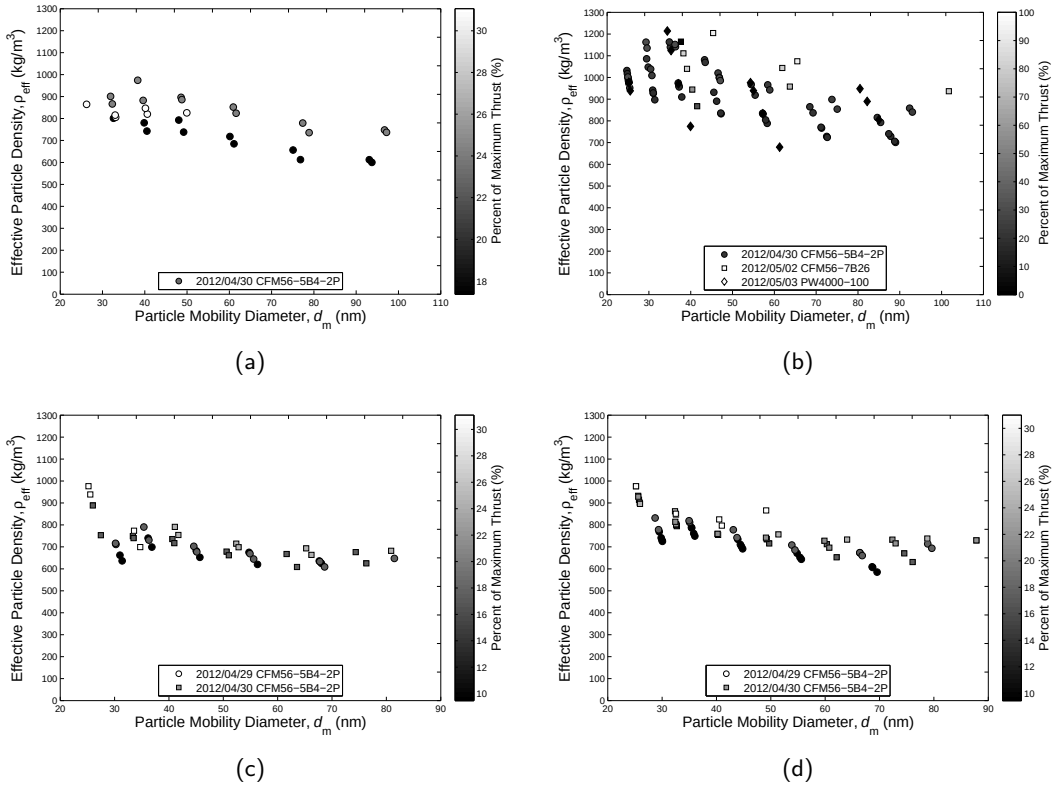

Figure 3-6: Effects of thrust and different engines on effective density functions measured from: (a) Annex 16 Undiluted Line, Denuded; (b) Annex 16 Undiluted Line, Undenuded; (c) Diluted Line B, Denuded; (d) Diluted Line B, Undenuded.

Figure 3-6b also shows the effective densities from three different turbine engines: CFM56-5B4-2P, CFM56-7B26 and PW4000-100. These measurements also followed the trend that the effective density increased as engine thrust increased. Furthermore, the effective densities produced by these two other engines were similar to the CFM56-5B4-2P engine results.

Figure 3-7 shows all of the results from the denuded, diluted line or the nvPM effective densities measured across all of the CFM56-5B4-2P engine load points. The shaded region shown in Figure 3-7 outlines the standard error of the mass-mobility fit, as described previously, and was determined to be ± 55 kg/m^3. Therefore, due to the small variation in nvPM effective density from engine thrust, the nvPM effective density function of aircraft exhaust can be approximated by:

$$\rho_{\text{eff}} = 11.92 d_{\text{m}}^{2.76-3} \pm 55, \tag{3.1}$$

where d_{m} is in m and ρ_{eff} is in kg/m^3.

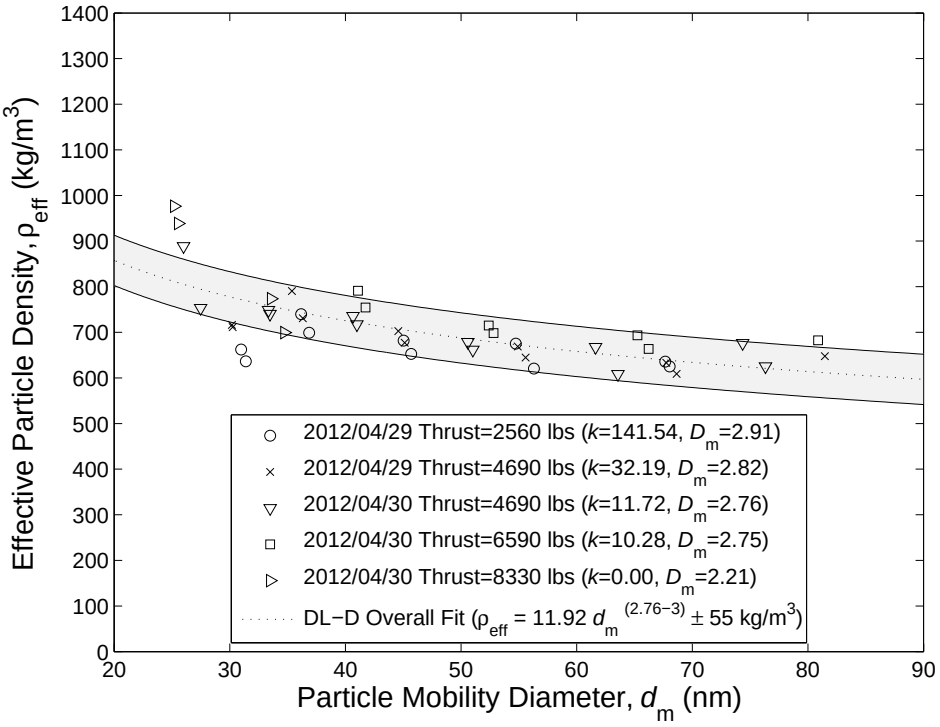

Figure 3-7: Average non-volatile effective density, measured on Diluted Line B, Denuded, from a CFM56-5B4 turbine engine across all measured load points.

3.2.3 Non-volatile particulate matter mass concentration comparisons

Applying the measured diluted, denuded effective density functions to the mobility size distributions measured at the same conditions, the nvPM mass concentrations produced by the CFM56-5B4-2P engine were determined. The CPMA-mDMS, LII and MSS all measured from Diluted Line B, however the mobility size distributions were measured on Diluted Line A. Therefore to approximate the mobility size distributions in Diluted Line B from Diluted Line A some assumptions were made. The losses in Diluted Line B and Diluted Line A were assumed to be equal and the dilution factor of each line was accounted for by calculating the real-time dilution ratios from the raw and diluted CO_2 concentrations. The losses in the AVL volatile particle remover (VPR) were neglected and the dilution ratio with the VPR was assumed to be constant at the value determined at the beginning of the campaign.

Furthermore no denuded mobility size distributions were measured on April 30th. Therefore these denuded size distributions were approximated by matching engine conditions (engine thrust and exhaust exit temperature) from April 29th to April 30th. These assumptions were applied to the mobility size distributions measured by a long SMPS and a nano SMPS. The nano SMPS only characterized a portion of the total mobility size distribution as it only measured particles up to 63.8 nm, but the count median diameter (CMD) of the aircraft mobility size distribution was 20 nm to 40 nm. This limitation was accounted for by fitting a lognormal curve to the nano SMPS data through Chi-Squared minimization and calculating the mass concentration from this fit (nano SMPS fitted). The nvPM mass concentrations calculated using these assumptions are shown in Figure 3-8.

The nano SMPS was found on average to underestimate the nvPM mass concentration by 20.3% relative to the LII on April 29th and 40.5% relative to the LII on April 30th. This result was expected as the nano SMPS did not consider the entire mobility size distribution. The long SMPS and nano SMPS fitted were found on average to overestimate the nvPM mass concentration by 71.3% and 92.0% relative to the LII on April 29th and 22.4% and 52.6% relative to the LII on April 30th respectively. This disagreement was likely caused by the assumptions made to approximate the non-volatile mobility size distribution, such as dilution ratios, particle losses and matching engine conditions. The disagreement between the LII and MSS was found to be negligible.

In the future an SMPS or DMS should sample the same denuded exhaust as other mass instruments so a better comparison can be completed. Previous studies with diesel soot have shown that a DMS is capable of measuring mass concentrations with a known density function (Symonds et al., 2007). These measurements are expected to be within 32% of the true value, determined by propagating the DMS uncertainty of 10% (Symonds, 2010) with the effective density function uncertainty of 10.4% (Johnson et al., 2013b).

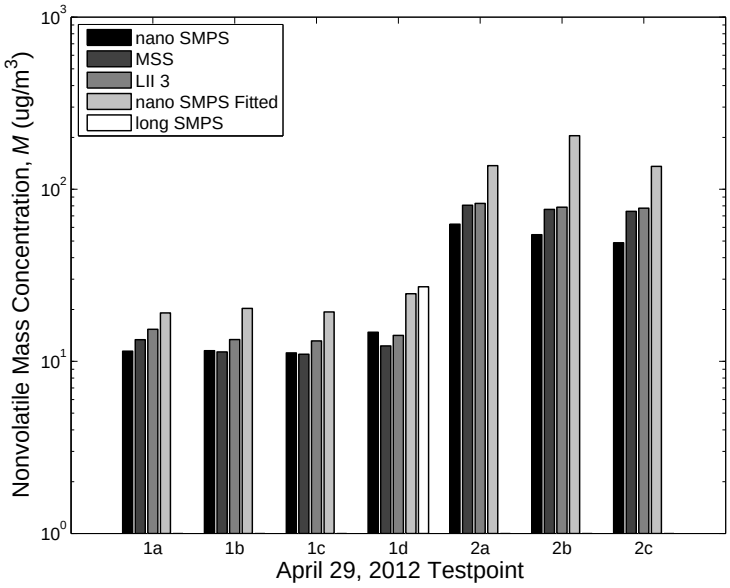

(a)

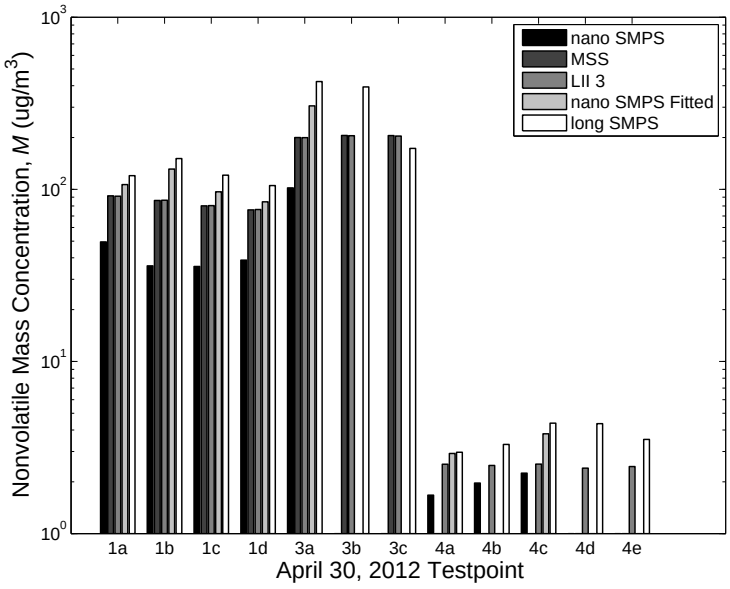

(b)

Figure 3-8: Non-volatile mass concentration from integrating the effective density function over the mobility size distribution and comparing to other mass concentration measurement techniques such as the LII and MSS.

Bibliography

Anderson, B., Cofer, W., Barrick, J., Bagwell, D., and Hudgins, C. (1998). Airborne observations of aircraft aerosol emissions ii: factors controlling volatile particle production. *Geophysical Research Letters*, 25(10):1693 – 1696.

Biskos, G., Reavell, K., and Collings, N. (2005). Description and theoretical analysis of a differential mobility spectrometer. *Aerosol Science and Technology*, 39(6):527–541.

Boies, A. (2013). Experimental evaluation of particulate matter morphology from gas turbines. In-preparation.

Crayford, A., Johnson, M., Marsh, R., Sevcenco, Y., Walters, D., Williams, P., Petzold, A., Bowen, P., Wang, J., and Lister, D. (2012). SAMPLE III: Contribution to aircraft engine PM certification requirement and standard Second Specific Contract- Final Report. Technical report, European Aviation Safety Agency (EASA).

Dakhel, P. M., Lukachko, S. P., Waitz, I. A., Miake-Lye, R. C., and Brown, R. C. (2007). Postcombustion evolution of soot properties in an aircraft engine. *Journal of Propulsion and Power*, 23(5):942 – 948.

Figliola, R. S. and Beasley, D. E. (2010). *Theory and Design for Mechanical Measurements*. John Wiley & Sons, Inc., 5th edition.

Johnson, T., Olfert, J., Symonds, J. P., , Johnson, M., Swanson, J., Thomson, K., Smallwood, G. J., Crayford, A., and Boies, A. (2013a). Effective density and mass-mobility exponent of aircraft particulate matter. *Journal of Propulsion and Power*, In-preparation.

Johnson, T. J., Symonds, J. P., and Olfert, J. S. (2013b). Mass-mobility measurements using a centrifugal particle mass analyzer and differential mobility spectrometer. *Aerosol Science and Technology*, 47(11):1215–1225.

Liscinsky, D. and Hollick, H. (2010). Effect of particle sampling technique and transport on particle penetration at the high temperature and pressure conditions found in gas turbine combustors and engines. *NASA contractor report, NASA/CR-2010-NNC07CB03C*.

Olfert, J. and Collings, N. (2005). New method for particle mass classification - the Couette centrifugal particle mass analyzer. *Journal of Aerosol Science*, 36(11):1338–1352.

Olfert, J. S., Symonds, J. P. R., and Collings, N. (2007). The effective density and fractal dimension of particles emitted from a light-duty diesel vehicle with a diesel oxidation catalyst. *Journal of Aerosol Science*, 38(1):69–82.

Park, K., Kittelson, D., Zachariah, M., and McMurry, P. (2004a). Measurement of inherent material density of nanoparticle agglomerates. *Journal of Nanoparticle Research*, 6(2):267–272.

Park, K., Kittelson, D. B., and McMurry, P. H. (2004b). Structural properties of diesel exhaust particles measured by transmission electron microscopy (tem): Relationships to particle mass and mobility. *Aerosol Science and Technology*, 38(9):881 – 889.

Peck, J., Timko, M. T., Yu, Z., Wong, H.-W., Herndon, S. C., Yelvington, P. E., Miake-Lye, R. C., Wey, C., Winstead, E. L., Ziemba, L. D., and Anderson, B. E. (2012). Measurement of volatile particulate matter emissions from aircraft engines using a simulated plume aging system. *Journal of Engineering for Gas Turbines and Power*, 134(6).

Reavell, K., Hands, T., and Collings, N. (2002). A fast response particulate spectrometer for combustion aerosols. Technical Report SAE 2002-01-2714.

Swanson, J. (2013). Characterization of solid and semi-volatile gas-turbine particulate matter using a catalytic stripper. In-preparation.

Symonds, J. P. R. (2010). *Calibration of fast response differential mobility spectrometers*. Metrology of Airborne Nanoparticles, Standardisation and Applications (MANSA), National Physical Laboratory (NPL), London, UK, June 8-9, 2010.

Symonds, J. P. R. and Reavell, K. (2007). *Calibration of a Differential Mobility Spectrometer*. European Aerosol Conference, Salzburg, Austria, September 9-14, 2007.

Symonds, J. P. R., Reavell, K. S., and Olfert, J. S. (2013). The cpma-electrometer system- a suspended particle mass concentration standard. *Aerosol Science and Technology*, 47(8):i–iv.

Symonds, J. P. R., Reavell, K. S. J., Olfert, J. S., Campbell, B. W., and Swift, S. J. (2007). Diesel soot mass calculation in real-time with a differential mobility spectrometer. *Journal of Aerosol Science*, 38(1):52–68.

Timko, M., Yu, Z., Onasch, T., Wong, H.-W., Miake-Lye, R., Beyersdorf, A., Anderson, B., Thornhill, K., Winstead, E., Corporan, E., Dewitt, M., Klingshirn, C., Wey, C., Tacina, K., Liscinsky, D., Howard, R., and Bhargava, A. (2010). Particulate emissions of gas turbine engine combustion of a fischer-tropsch synthetic fuel. *Energy and Fuels*, 24(11):5883 – 5896.

Wiedensohler, A. (1988). An approximation of the bipolar charge distribution for particles in the submicron size range. *Journal of Aerosol Science*, 19:387–389.

Chapter 4

General Discussion and Conclusions

A novel measurement system was developed, a CPMA-DMS system, which is capable of measuring the transient mass-mobility of individual nano-particles at one mass setpoint or characterize the entire effective density function in a fraction of the time compared to previous measuring systems. The results of this system must be corrected for the effects of uncharged and multiply-charged particles. This correction was applied by developing a code in Matlab. This instrument configuration and correction method has never been used anywhere else in the world.

Two different CPMA-DMS systems and the multiple-charge correction method were validated by measuring the effective density of DEHS. DEHS was used as it has a known and size-independent density of 912 kg/m^3. The CPMA-mDMS system measured an effective density of 964 kg/m^3 or within 5.7% of the accepted value, while the CPMA-sDMS system measured 1027 kg/m^3 or within 12.6% difference of the accepted value. It was found both the multiple-charge correction and size calibration were significant, each causing a maximum change in effective density greater than 10%, for either system. Therefore, both the multiple-charge correction and size calibration must be applied to obtain accurate results from the CPMA-mDMS or CPMA-sDMS system. The uncertainty in effective density, assuming a 95% confidence interval, was 9.5–10.4% for the CPMA-mDMS system depending on particle

A version or portion of this chapter has been submitted for publication/accepted for publication/published. Accepted: Johnson et al. (2013b), Submitted: Johnson et al. (2013a)

mobility size and 30.1% for the CPMA-sDMS system. While these uncertainties are higher than previously described mass-mobility measurement techniques, a CPMA-DMS system can measure transient sources at one particle mass or determine a complete aerosol density distribution in minutes from steady state sources.

A CPMA-mDMS system was then used to measure the size-resolved effective density of aircraft particle matter. This characteristic had only previously been measured as a mass weighted average and therefore could not accurately convert measured mobility size distributions to mass distributions.

The mass-mobility exponent was found to be between 2.72 and 2.82 for varying CFM56-5B4-2P engine load points, with only a few exceptions. These outliers were thought to be caused from measuring only a very narrow range of the effective density function or from the CPMA classifying multiple species, thus generating a peak in the effective density function. These high mass-mobility exponents could indicate that aircraft particulate matter is more spherical than traditional combustion sources, such as flames or diesel engines. The shift in effective density between the denuded and undenuded sample of 45.8 kg/m^3 on the diluted line and 191.4 kg/m^3 on the undiluted line. This shift indicates the presence of some volatile material and that a volatile component remover, such as a catalytic stripper, volatile particle remover (VPR) or thermodenuder, must be used to denude the volatile fraction if future regulations require the measurement (mass or number concentration) of only the non-volatile particulate matter. The effective particle densities from CFM56-7B26 and PW4000-100 engines were similar to the CFM56-5B4-2P and all three engines show the same trend that effective density increased as engine thrust increased. The change in effective density due to engine thrust was found to be the smallest on the diluted line and largest on the undiluted line. This small deviation in the nvPM effective density allowed it be approximated using a mass-mobility prefactor of 11.92 and exponent of 2.76, with a 95% confidence interval of 55 kg/m^3. The mass concentrations determined using the effective density functions and mobility size distributions were found to agree within an average of 59.6% with the LII, even though many assumptions were made to approximate the mobility size

distributions. In the future the denuded mobility size distributions and mass concentrations, measured using a LII and MSS, should be completed under the same sampling system so that a more comprehensive comparison can be made.

Bibliography

Johnson, T., Olfert, J., Symonds, J. P., , Johnson, M., Swanson, J., Thomson, K., Smallwood, G. J., Crayford, A., and Boies, A. (2013a). Effective density and mass-mobility exponent of aircraft particulate matter. *Journal of Propulsion and Power*, In-preparation.

Johnson, T. J., Symonds, J. P., and Olfert, J. S. (2013b). Mass-mobility measurements using a centrifugal particle mass analyzer and differential mobility spectrometer. *Aerosol Science and Technology*, 47(11):1215–1225.